Atmospheric CO_2 exchanges dynamics over a temperate tidal marsh

Camille PERY

M2 Dynea

2023-2024

Université de Pau et des Pays de l'Adour

IFREMER - Resources and Environment Laboratory of the Pertuis Charentais (LER-PC)

RESUME

Les écosystèmes côtiers végétalisés sont encore sous-représentés dans les études régionales/mondiales sur le cycle et les flux du carbone. Malgré leur faible superficie, ils représentent une part importante de la productivité mondiale annuelle des océans (vasières, jusqu'à 20%), du carbone stocké sur Terre et des flux de CO_2 air-mer (zones humides, 17%). Dans le contexte de l'augmentation des émissions de gaz à effet de serre, du changement climatique et de l'atténuation de ses effets, il est primordial d'accroître les approches intégratives et multidisciplinaires pour mieux comprendre les processus, la dynamique des flux et les facteurs de contrôle aux interfaces d'échanges terrestres-aquatiques-atmosphériques aux différentes échelles spatio-temporelles. Dans cet objectif et dans le cadre du projet La Rochelle Territoire Zéro Carbone (LRTZC 2019-27), la dynamique du carbone a été étudiée au sein d'un système de marais tempéré (baie de l'Aiguillon, littoral atlantique français) et de ses zones d'habitat pré salé - vasières, colonisées respectivement par des plantes halophytes et des communautés microphytobenthiques, susceptibles d'influencer les processus et flux de carbone associés. Une station atmosphérique d'Eddy Covariance a été déployée avec des mesures saisonnières *in situ* simultanés au sein des différents compartiments (air, sol/sédiments, eau) et des interfaces associées pour caractériser temporellement et spatialement les échanges de CO_2 atmosphérique et les facteurs de contrôle. Le bilan carbone du système de marais littoraux étudié a révélé une absorption nette de CO_2 atmosphérique de -285 $gC\ m^{-2}\ an^{-1}$ (-10,5 $tCO_2eq.ha^{-1}.an^{-1}$), avec des valeurs de flux spécifiques provenant des zones d'habitat vasières et pré salé de -430 et -156 $gC\ m^{-2}\ an^{-1}$ (-15,8 et -5,7 $tCO2eq.ha^{-1}.an^{-1}$), respectivement. Une grande variabilité des flux a été observée aux différentes échelles de temps, c'est-à-dire annuelles, saisonnières, tidale et diurnes. La vasière a agi comme un puits de CO_2 pendant la journée en raison de l'intense activité de production primaire de MPB, en particulier au printemps et en été, et est devenue une source de CO_2 la nuit en raison de la respiration. La forte variabilité des flux diurne a été influencée par des paramètres environnementaux tels que la température (nuit) et le rayonnement photosynthétiquement actif (PAR, jour) principalement. Le rythme des marées a également influencé la dynamique des flux, avec des flux plus négatifs pendant les marées basses de vive-eaux pendant la journée, soulignant l'importance de l'irrigation des vasières (marée, pluie) ainsi que sur l'activité photosynthétique. Ces mesures et résultats obtenus dans la présente étude ont participé à une meilleure compréhension des processus/flux de carbone des écosystèmes de carbone bleu sous-étudiés en France et ailleurs et ont été discutés en détail à partir de considérations méthodologiques et du bilan carbone du système de marais étudié dans le contexte du changement climatique.

ABSTRACT

Vegetated coastal ecosystems are still under represented in regional/global carbon cycling and flux studies. Despite their small surface area, they represent a significant part in annual global ocean productivity (mudflats, up to 20%), carbon stored on Earth and in air-sea CO_2 fluxes (wetlands, 17%). In the context of rising greenhouse gas emissions, climate change and mitigation, it is paramount to increase integrative and multidisciplinary approaches to better understand processes, flux dynamics and controlling factors at terrestrial-aquatic-atmospheric exchange interfaces at the various spatiotemporal scales. In this objective and the framework of the La Rochelle Zero Carbon Territory project (LRTZC 2019-27), the carbon dynamic was studied within a temperate tidal marsh system (Aiguillon Bay, French Atlantic coast) and its marsh - mudflat habitat zones, colonized by halophytic plants and microphytobenthic communities respectively, likely to influence associated carbon processes and fluxes. An atmospheric Eddy Covariance station was deployed with simultaneous seasonal *in situ* measurements within the different compartments (air, soil/sediment, water) and associated interfaces to temporally and spatially characterize atmospheric CO_2 exchanges and controlling factors. The carbon budget of the studied tidal marsh system revealed a net uptake of atmospheric CO_2 of -285 gC m^{-2} yr^{-1} (-10.5 $tCO_2eq.ha^{-1}.an^{-1}$), with specific flux values from mudflat and marsh habitat zones of -430 and -156 gC m^{-2} yr^{-1} (-15.8 and -5.7 $tCO_2eq.ha^{-1}.an^{-1}$), respectively. High flux variability was observed at the different time scales, i.e. annual, seasonal, tidal and diurnal scales. The mudflat acted as a CO_2 sink during the day through intense MPB primary production activity, especially in spring and summer, and became a CO_2 source at night due to respiration. The strong diurnal flux variability was influenced by environmental parameters such as temperature (night-time) and photosynthetically active radiation (PAR, daytime) mainly. Tidal rhythm also influenced flux dynamics, with more negative fluxes during low spring tides during daytime, highlighting the importance of mudflat irrigation (tide, rain) as well on photosynthetic activity. These measurements and results obtained in the present study took part in the better carbon process/flux understanding of under studied blue carbon ecosystems in France and elsewhere and were discussed in details from methodological considerations and the carbon budget of the studied marsh system in the context of climate change.

ACKNOWLEGMENTS

First of all, I would like to thank Audrey Bruneau, manager of the LER PC laboratory, and Bénédicte Charrier, manager of the Ifremer La Tremblade station, for their warm welcome and for allowing me to spend my two master's years at the station.

I would now like to thank Pierre Polsenaere, who has supervised and followed my work with great kindness and consideration over the last two years. Thank you very much for allowing me to develop professionally throughout my master's degree. I'm also very grateful to you for giving me the opportunity to attend an international conference where we were both able to present our work. Thank you for everything.

I would like to take this opportunity to thank Christine, Lucila and Anais for their great advice and help during this conference and for the really good time we all had together in Vienna.

Thanks to Eric Lamaud (INRAe) for the many discussions we had and for his involvement in my work. Thank you for allowing me to improve the rigour and relevance of each of my analyses.

I would like to extend my warmest thanks to the other members of the Laboratoire Environnement et Ressources des Pertuis Charentais, as well as the members of the Unité Adaptation et Santé des Invertébrés Marins, the Plateforme Expérimentale Mollusques Marins La Tremblade and all the staff at the station.

Finally, I'd like to thank Pierre and Jules who have been a great moral support the last few months through all the great times we've shared. Thank you both.

1. Introduction

The global CO_2 budget includes all natural and anthropogenic CO_2 exchanges between the different involved reservoirs, i.e. atmospheric, oceanic and continental compartments. These exchanges reflect underlying natural processes such as photosynthesis, respiration, decomposition and combustion, as well as interactions with human activities such as fossil fuel combustion and deforestation. The global carbon cycle has been greatly disrupted by industrialization. Since the transition from the pre-industrial to the industrial era, greenhouse gas emissions have increased, as atmospheric CO_2 concentrations from around 270 ppm in 1750 to 420 ppm in 2023 (Friedlingstein et al. 2023). According to Intergovernmental Panel on Climate Change (IPCC) reports, rising CO_2 concentrations in the atmosphere are contributing to global warming and environmental changes (rising sea levels, ocean acidification, extreme events) (IPCC, 2023).

The coastal zone represents a clear and dynamic interface within global/regional carbon cycles, involving numerous vertical and horizontal carbon processes and exchanges in and between the three compartments. Defined as the oceanic area located on the continental shelf including the entire tidally influenced surface down to a depth of 200 meters (Polsenaere 2011, Bauer et al. 2013), the coastal zone represents only 7% of the surface of the global ocean (i.e. about $30x10^6$ km²). However, this area performs important ecological functions such as primary production, up taking globally between 0.22 and 0.45 Pg C yr^{-1} (1 PgC = 10^{15} gC) and accounting for 14 to 30% of the total primary production (Gattuso et al. 1998; G. G. Laruelle et al. 2013; Regnier et al. 2013; Roobaert et al. 2019).

Specifically, coastal ecosystems, comprising estuaries, mangroves, salt marshes, and continental shelves, play a crucial role in atmospheric CO_2 exchanges (captation) and carbon sequestration (Gattuso et al. 1998). These ecosystems serve as both sources and sinks of atmospheric CO_2 through complex processes (as cited above) operating at different spatial and temporal scales (Cai 2011). Estuaries generally release (source) CO_2 to the atmosphere (~0.25 Pg C y^{-1}) due to the decomposition of organic carbon (OC) and nutrient inputs (Cai 2011; Laruelle et al. 2010). Upper estuaries are strong sources (39 ± 56 molC m^{-2} yr^{-1}), contrary to lower estuaries which correspond to weaker sources (8.4 ± 14 molC m^{-2} yr^{-1}) (C.-T. A. Chen et al. 2013). At the opposite, continental shelves globally uptake (sink) CO_2 from the atmosphere (~0.25 Pg C y^{-1}) due to intense primary production rates (Cai 2011; Laruelle et al. 2010). Here as well, climate change can shift coastal ecosystems from being net sinks to sources of CO_2. Rising temperatures, altered precipitation patterns and human activities, such as land use and pollution, can reduce carbon sequestration capacity of theses ecosystems and increase CO_2 emissions (Duarte et al. 2021; Macreadie et al 2013; Z. L. Chen et Lee 2022). Despite the significance of the coastal zone in regional/global carbon budgets, our understanding of how climate change will impact coastal carbon dynamics remains limited and needs to be thorough (Mcleod et al. 2011; Cai 2011).

Vegetated coastal ecosystems, known as “Blue Carbon” ecosystems, such as tidal marshes, seagrasses, and mangroves, are particularly effective in carbon captation and sequestration (Mcleod et al. 2011; Mayen et al. 2024). These ecosystems are increasingly recognized for their potential to contribute to climate change mitigation and adaptation (Macreadie et al. 2021). Tidal marshes, which are prevalent in middle to high latitudes, highlight the role of Blue Carbon ecosystems (Mcowen et al. 2017). They generally act as net CO_2 sinks in temperate and high latitudes, whereas in subtropical and tropical regions, they tend to be net CO_2 sources due to warmer temperatures and higher organic carbon inputs (Borges et al. 2005; Regnier et al. 2013; Cai et al. 2006). Tidal marshes are situated at the interface between terrestrial and oceanic compartments, connecting fresh and saline water

systems. These ecosystems are essentially composed, in the upper part, of halophytic plants adapted to regular tidal immersion (Mcowen et al. 2017). The carbon dynamics in these regions are further influenced by the transport of carbon from inland terrestrial ecosystems to downstream coastal systems and then to the ocean, a process that represents a crucial component of the global carbon cycle (Regnier et al. 2013). The lower zone of tidal marshes is composed by a muddy unvegetated system (Mcowen et al. 2017). Mudflats are colonized by microphytobenthos communities recognized as important primary producers at the bottom of trophic food webs in tidal mudflats. Only a few studies have highlighted the importance of unvegetated coastal areas, such as mudflats, in regional/global carbon cycle. However, recent studies reveal that non-vegetated mudflats have carbon sequestration rates comparable to those of vegetated coastal ecosystems, notably due to a high sedimentation rate (J. Chen et al. 2020; Z. L. Chen et Lee 2022). This land-ocean continuum then represents a succession of different habitats colonized by various organisms. It is also a continuum of chemically and physically active biogeochemical systems, all interconnected and essential for the processing, transport, atmospheric exchanges and sequestration of carbon. CO_2 dynamics in intertidal marshes are mainly determined by a combination of biological activity, tidal action, sediment interactions and environmental conditions, acting on different temporal and spatial scales (Morris et al. 2013). These processes are driven by tidal cycles, which cause periodic flooding and drainage, as well as diurnal and seasonal variations. During the day, photosynthetic activity tends to dominate leading to greater CO_2 uptake, while due to lack of light respiration increases at night often resulting in net CO_2 releases (Mayen et al. 2024). Environmental conditions and plant phenology determine seasonal variations in marsh CO_2 fluxes, with bright, warm seasons generally favoring biological activity. Moreover, sediment interactions, such as carbon burial and release, are influenced by the movement of tidal water, which transports organic and inorganic carbon through the tidal marsh (Wang et Cai 2004; Chmura 2013). Understanding the interactions along this continuum provides a better understanding of regional/global carbon cycles and can help predicting the impact of climate change on coastal carbon dynamics.

To accurately and in an integrative manner measure CO_2 flux dynamic in tidal marshes and associated terrestrial/aquatic/atmospheric compartments and habitats, it's necessary to use a combination of different techniques. The atmospheric Eddy Covariance (EC) method permits to capture high frequency fluxes at the global ecosystem scale, providing continuous measurements of CO_2 exchanges between a surface (i.e. canopy, sediments or water) and the atmosphere (Baldocchi 2003). This technique is recognized for its ability to offer precise flux measurements in heterogenous intertidal systems at both terrestrial and aquatic interfaces (Laurila et al. 2012; Polsenaere et al. 2012; Mayen et al. 2024). Additionally, benthic chambers assess CO_2 fluxes at emersion at the community scale. These chambers allow for the isolation and analysis of benthic community respiration and photosynthesis processes (Migné et al. 2004). During immersion periods, CO_2 partial pressures (pCO_2) sensors can automatically measure pCO_2 in the water column, enabling the assessment of CO_2 dynamics at the water-atmosphere interface. This approach has been validated in various marine and freshwater studies (Borges et Frankignoulle 2003; Mayen et al. 2023; Berg et al. 2019). Then, the integration of these different coupling methods provides a comprehensive assessment of CO_2 processes and fluxes across the different temporal (diurnal, tidal, seasonal, annual) and spatial (marsh, mudflat) scales, enhancing our understanding of the complex biogeochemical processes in intertidal zones such as tidal marshes.

The present study aims to characterize the dynamic of atmospheric CO_2 fluxes and associated physico-chemical and biological processes in a temperate intertidal bay system comprising a typical marsh – mudflat continuum. The Bay of Aiguillon constitutes a highly representative and workshop area to study CO_2 dynamics in a typical intertidal marsh system. It features a well-defined continuum between marsh and mudflat zones connected through

estuarine and channel waters, allowing the study of carbon fluxes across different intertidal habitats and compartments. By establishing the carbon balance (i.e. sources and sinks of atmospheric CO_2) for this tidal marsh, the present study described processes involved at the different time scales (diurnal, tidal, seasonal, annual) within this marsh – mudflat continuum at the ecosystem scale which is crucial for directing sustainable coastal zone management practices.

2. Materials and Methods

2.1. Study site

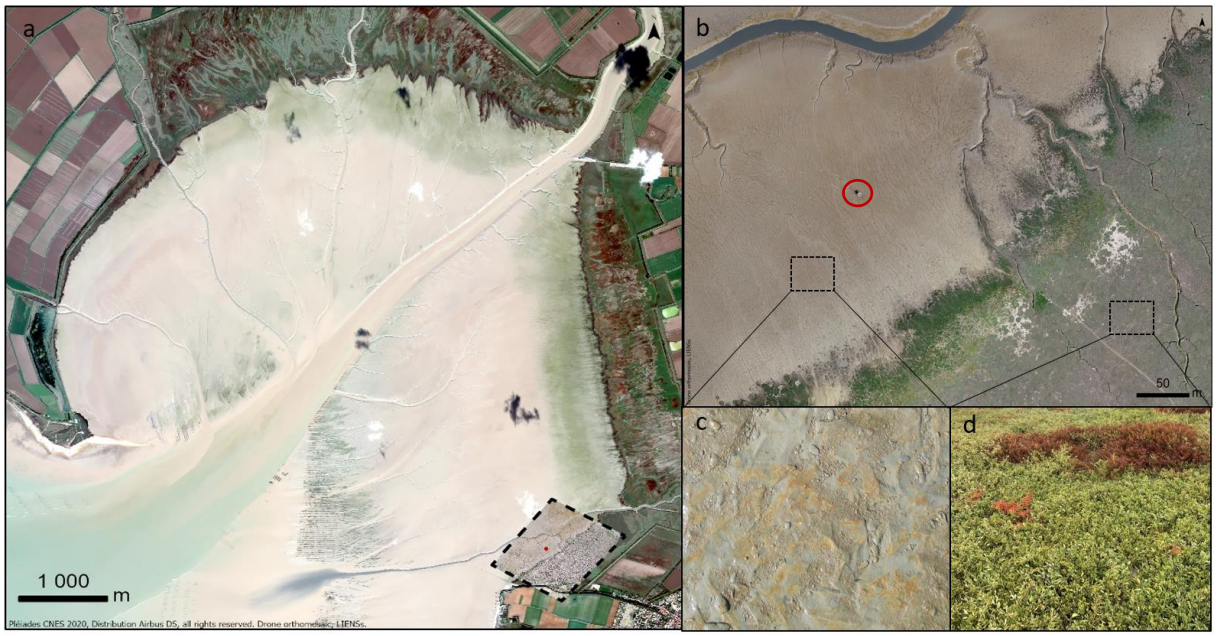

Figure 1. The bay of Aiguillon (a) with at the southwest, the studied site (dotted boxes represent field work locations). The studied site (b) composed by mudflat (c) and marsh areas (d). The Eddy Covariance station is circled in red.

The bay of Aiguillon is a coastal bay located on the Atlantic coast, up north La Rochelle city (western France). It is a part of the Charentais Sounds representing a perfect transition between continental and oceanic compartments. The bay is an intertidal area with mudflats bordered by marshes and supplied with freshwaters connected to 6350 km² of watersheds (Polsenaere et al. 2019, Coignot et al. 2020, Deborde et al. 2021) (Fig. 1). Marshes of the bay are among the largest in France with an area of 1200 ha. Associated with a mud area of 3 700 ha, the total area of the bay reach 4 900 ha (Godet et al. 2015; Plan de gestion RNN 2023). The ecological importance of theses marshes associated with these extensive mudflats, has led to the establishment of a National Natural Reserve on December 30, 1996. The Reserve spans the departments of Vendée (85) and Charente-Maritime (17). In Charente-Maritime, the reserve is managed by the League for the Protection of Birds (Ligue pour la Protection des Oiseaux, LPO), while in Vendée, it is managed by the French Biodiversity Office (Office Français de la Biodiversité, OFB). The bay of Aiguillon is also protected under the Natura 2000 network. This has resulted in special legislation and management to ensure the protection of this critical and fragile ecosystem.

The tidal marsh studied here comprises different connected zones: the schorre, composed of marshes, which are vegetated by halophilous plants, and the slikke, corresponding to the mudflat, without any vegetation but colonized by microphytobenthos (Herlory et al.

2004). The microphytobenthos is an essential component of the trophic network and primary production. It represents the basis of the trophic network and provides a fundamental food source for various benthic organisms, such as meiofauna and macrofauna (Christianen et al. 2017). It accounts for a large proportion of total primary production in intertidal zones (MacIntyre et al. 1996). This high productivity supports a rich and diverse community of invertebrates and fish, which themselves support higher trophic levels, such as birds and other predators (Kritzer et al. 2016). The schorre itself is zoned according to the different vegetation communities. The higher schorre hosts a diverse array of vegetation, the middle schorre is characterized by *Halimione*, and the lower schorre is initially colonized by *Salicornia* and *Spartina*. These zones are closely linked to the tidal regime, with the lower schorre and slikke regularly submerged during high tides. This tidal inundation gradient determines the distribution of vegetation and corresponding biological communities, with the intensity and frequency of submersion influencing the productivity and composition of each zone.

The bay of Aiguillon is subject to semi-diurnal tides but is not exposed to significant wave action, and current speeds are reduced, resulting in continuous sediment deposits. The average sedimentation rate in the bay is + 1.17 ± 0.38 cm yr^{-1} (from 2010 to 2021), one of the highest sedimentation rates in the world (Amann et al. 2023). This sediment accumulation allows the schorre to expand, providing a substrate for vegetation to develop and colonize the new sediment-rich soil. Over the past 40 years, the schorre has grown by approximately 7 hectares per year progressing over the mudflat. Oceanic water reaches marsh habitats at spring tides only for tidal coefficients greater than 70. The primary use of the schorres in the bay of Aiguillon is for cutting, especially *Puccinellia maritima* though the southeastern studied area, south of the Canal du Curé, has never been cut and influenced by theses anthropogenic practices (Godet et al. 2015, Plan de gestion RNN 2023).

The study site is part of the La Rochelle agglomeration as this study is being integrated into the LRTZC project. The La Rochelle Zero Carbon Territory (LRTZC) project, led by the La Rochelle Agglomeration, the city and the University of La Rochelle, aims to achieve carbon neutrality in La Rochelle by 2040. The project focuses on reducing CO2 emissions through mitigation, climate adaptation and carbon sequestration.

2.2. Atmospheric CO_2 exchanges measured at the global ecosystem scale by Eddy Covariance method and associated meteorological data measurements

2.2.1. Eddy Covariance data acquisition

The atmospheric Eddy Covariance technique is a micrometeorological method that quantifies net CO_2 fluxes at the ecosystem-atmosphere interface. In the atmosphere, CO_2 is transported by numerous homogeneous eddies of varying size and frequency. These eddies are located in the surface boundary layer. This method relies on capturing, within these eddies, the covariance between vertical wind speed (w), air density (ρ), and the dry mole fraction of the gas of interest (s), which can be expressed as:

$$F = \overline{\rho w s} \approx \overline{\rho w' s'}$$

where the overbar indicates the time averaging and the prime represents fluctuations around this average (Reynolds 1886; Burba 2013). In this study, measured fluxes were averaged every 10 minutes due to strong flux fluctuations at the tidal scale (Polsenaere et al. 2012; Van Dam et al. 2021, Mayen et al. 2024). Negative CO_2 fluxes indicate the ecosystem acts as a CO_2 sink, while positive fluxes indicate it is a source. Fluxes are given in µmol m^{-2} s^{-1}.

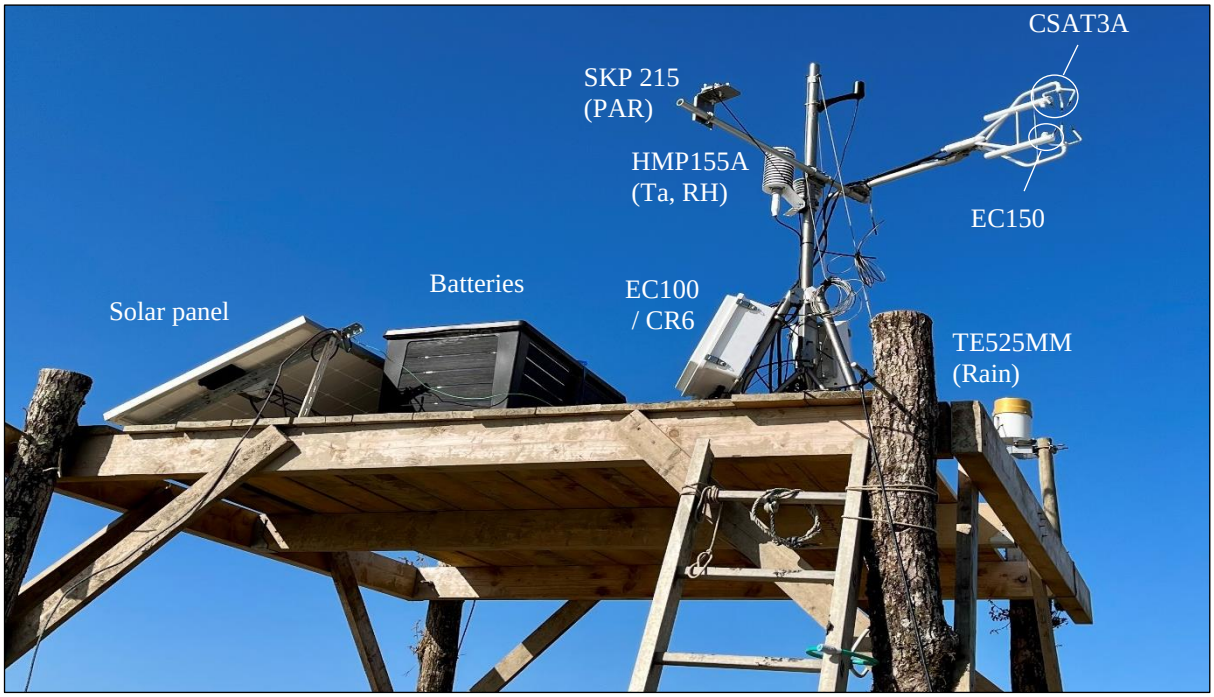

Figure 2. The Eddy Covariance station set-up with the two main anemometer and CO_2 EC sensors (CSAT3A and EC150) linked to EC100 electronics module connected to the data acquisition central (CR6), with the associated environmental sensors (HMP155A, SKP 215 and TE525MM). The system is powered by batteries charged by solar panels.

An EC station (Campbellsci) was installed in January 2023 at the southwest of the bay of Aiguillon, at the edge between the marsh downstream and the mudflat upstream (100 meters downstream from the marsh, Fig. 1). The station includes several key sensors set at a height of 5 meters above the sediment at low tide. The sensors are positioned at the top of a 2m tower, itself installed on a 3m high platform (Fig. 2). These sensors include an ultrasonic anemometer (CSAT3A) that measures three-dimensional wind speed components, and an open-path infrared gas analyzer (EC150, connected to the EC100 central) that measures CO_2 and H_2O concentrations in the air both at a frequency of 20 Hz. The tower is also composed by additional sensors measuring various environmental parameters every 10 minutes: a photosynthetically active radiation (PAR) sensor (SKP215), an air temperature and relative humidity sensor (HMP155A), and a rainfall sensor (TE525MM, Texas Electronics). Soil temperature and water content is measured by two probes (CS655), one in the mudflat and the other in a patch of *Spartina*. The data acquisition system is powered by two batteries (12 volts, 260 Ah) charged by monocrystalline solar panels (24 V, 200Wp module with MPPT 100 V/30 A controller; Victron Energy). High-frequency data were recorded on an SD micro-card and replaced every two weeks along sensor cleaning. Meteorological data were stored in the central acquisition system (CR6 datalogger, Campbell Scientific) (Fig. 2).

2.2.2. EC data processing and filtering

Raw EC data were processed using the EddyPro software (EddyPro® v7.0.8, LI-COR Inc.) to ensure accurate CO_2 flux measurements. Following Vickers and Mahrt (1997) and adapted methods for coastal systems by Polsenaere et al. (2012), Van Dam et al. (2021) and Mayen et al. (2024), the processing included several key steps: (1) unit conversion to check that the units for instantaneous data are appropriate and consistent to avoid any errors in the

calculation and correction of CO_2 fluxes; (2) despiking to remove outliers in the instantaneous data from the anemometer and gas analyzer due to electronic and physical noise and replaced the detected spikes with a linear interpolation of the neighboring values; (3) amplitude resolution to identify situations in which the signal variance is too low with respect to the instrumental resolution; (4) double coordinate rotation to align the x axis of the anemometer to the current mean streamlines, nullifying the vertical and cross-wind components; (5) time delay removal by detecting discontinuities and time shifts in the signal acquisition from the anemometer and gas analyzer; (6) detrending with removal of short-term linear trends to suppress the impact of low-frequency air movements; and (7) performing the Webb–Pearman–Leuning (WPL) correction to take into account the effects of temperature and water vapor fluctuations on the measured fluctuations in the CO_2 and H_2O densities (Burba 2013). CO_2 fluxes were calculated using the linear detrending method (Gash et Culf 1996) and averaged over 10-minute intervals. Data with more than 10% missing high-frequency data over these 10-minutes were excluded. Then, EddyPro software outputs contains 4.4% missing values. Additionally, some extreme values in data were identified and removed using the median absolute deviation (MAD) method (Papale et al. 2006). The MAD were calculated over a 2-week window separating daytime and night-time periods. Data above 5.2×MAD were removed. Without extreme values, the number of missing values reaches 10.6% from 01/02/2023 to 31/01/2024. Finally, data were filtered removing periods where friction velocity (u^*) values were less than 0,1 m s^{-1}. This parameter quantifies atmospheric turbulence then it permits to identify poorly mixed periods. The EC method often underestimates fluxes during these stable periods due to insufficient turbulent mixing. During these periods, the near-ground air can be decoupled from the air above, leading to an accumulation of CO_2 that is not exactly captured by measuring instruments (Barr et al. 2013; Gu et al. 2005). This u^* filter optimizes the accuracy of EC measurements particularly during night. After this last filtration the dataset contains a total of 28.2% missing values.

2.2.3. Footprint estimation from EC data and surface calculations from satellite images

The footprint, corresponding to the area around the EC station that contributes to the measured fluxes, was estimated with the Kljun et al. (2015) model. The footprint is calculated using the constant measurement height (Zm = 5 m) offset by the corrected varying tidal water levels measured by the STPS probe, the constant displacement height (d = 0.1 m), mean wind velocities (u_mean, m s^{-1}), standard deviations of the lateral velocity fluctuations after rotation (sigma_v, m s^{-1}), the Obukhov length (L), friction velocities (u_star, m s^{-1}) and wind directions (°), measured by the station. This area can be calculated at different scales: monthly, seasonally or yearly scales (Fig. 3; Tab. 1; Annex 1).

The identification of monthly surface areas occupied by each habitat within the monthly corresponding footprints were also done (N. Volto, LIENSs) (Tab. 1) to couple atmospheric CO_2 fluxes and metabolic processes with habitats. Footprint images were georeferenced with IGN orthophoto at 20cm to then extract the georeferenced image contours. The widest contour line was reserved and divided into 8 wind sectors. Within the 8 sectors, a classification was performed using Sentinel-2 images, which have a spatial resolution of 10 m and a high temporal resolution, with a revisit time of 5 days. Classification was also verified by sampling different habitats in the field (see more details in Paschal 2023).

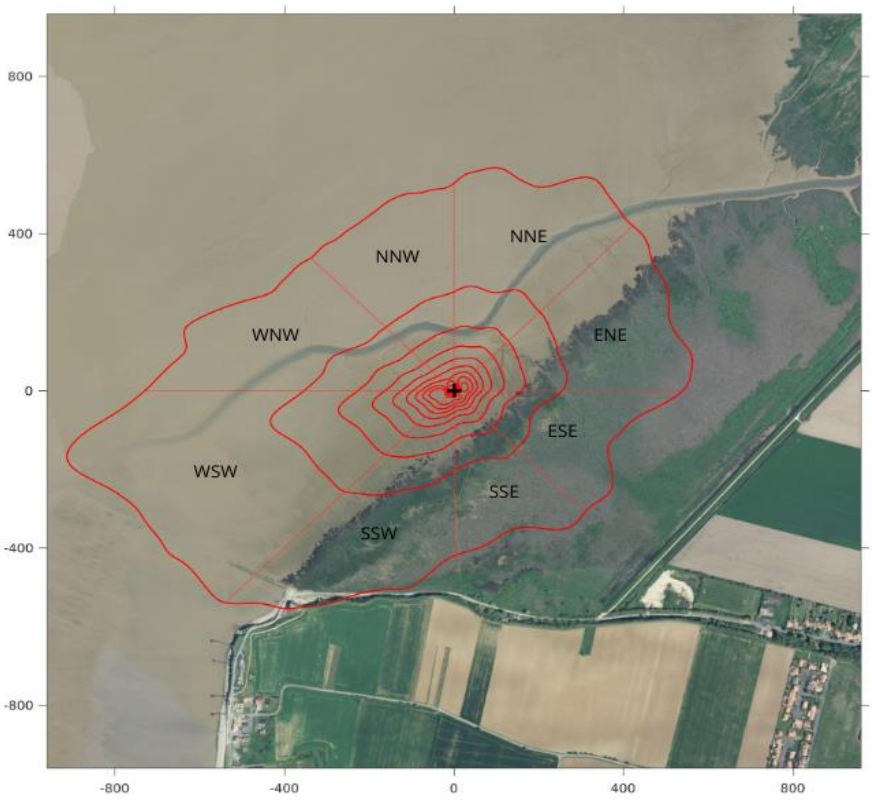

Figure 3. Mean annual EC flux footprint (01/02/2023 to 31/01/2024). Red contour lines represent the percentage contribution to measured fluxes from 10 to 90%. The EC station is represented by the black cross. The footprint covers 85.8ha. Dotted lines represent the division of the footprint into the 8 wind sectors. North-Northeast (NNE), East-Northeast (ENE), East-Southeast (ESE), South-Southeast (SSE), South-Southwest (SSW), West-Southwest (WSW), West-Nothwest (WNW) and Noth-Northwest (NNW).

Table 1. Surface areas (in hectare) of each habitat within the EC footprint computed for each month. In bold, the surface inside the 90% contour line of the monthly estimated footprint was used for surface habitat calculations.

	Jan	**Feb**	**Mar**	**Apr**	**May**	**Jun**	**Jul**	**Aug**	**Sep**	**Oct**	**Nov**	**Dec**
Puccinelia	1.7	1.7	1.7	1.7	1.0	0.1	0	0	1.7	1.7	1.4	1.7
Agropyron	0.5	0.2	0.4	0	0	0	0	0	0.6	0.7	0.2	1.2
Aster	5.0	4.9	4.0	4.9	3.3	1.5	0	0	4.2	4.2	2.0	4.3
Halimione	25.8	24.3	15.3	14.7	6.3	11.7	0	0	23.1	25.0	5.2	20.7
Salicornia	3.5	2.8	3.0	2.0	1.5	0.8	0	0	2.6	2.9	1.1	3.1
Spartina	3.3	3.3	2.3	3.2	2.9	1.4	0	0	2.6	2.8	1.5	2.7
Phragmites	0.1	0.1	0.4	0	0	0	0	0	0.1	0	0	0.4
Mud	54.9	61.8	49.4	77.2	69.7	6.0	23.2	12.5	54.2	41.2	14.7	53.8
Channel	2.2	2.2	3.0	4.0	3.6	0.2	2.1	0	3.1	1.9	0	2.3
NA	1.7	0.3	3.3	2.4	0	0	0	0.4	0.4	3.7	0.4	1.6
Total	**98.8**	**101.6**	**82.7**	**110.1**	**88.3**	**21.6**	**25.4**	**13.0**	**92.6**	**84.1**	**26.4**	**91.7**

2.2.4. EC data gap-filling and analysis

Missing values of the EC dataset (i.e. 28,2%) were gap-filled using a Random Forest (RF) model adapted for the present study. Breiman (2001) proposed a machine learning model which can build a non-linear relationship between a variable to be explained and several explanatory variables. Random forest is a learning method that constructs several decision trees during the training process and combines their results, using majority voting for classification or mean prediction for regression. This model mitigates overfitting and improves prediction accuracy by averaging the results of multiple trees, each built on random subsets of data (70%). This model's ability to process complex and non-linear relationships, such as those between CO_2 fluxes and the various associated environmental parameters, makes it adapted to the imputation of EC data missing values as done in the present study. That's why this kind of models is more and more used to gap-filled EC data (Kim et al. 2020; Cui et al. 2021; Mayen et al. 2024; Moffat et al. 2007). By the accurately estimating missing values, random forest improves the overall quality of the dataset.

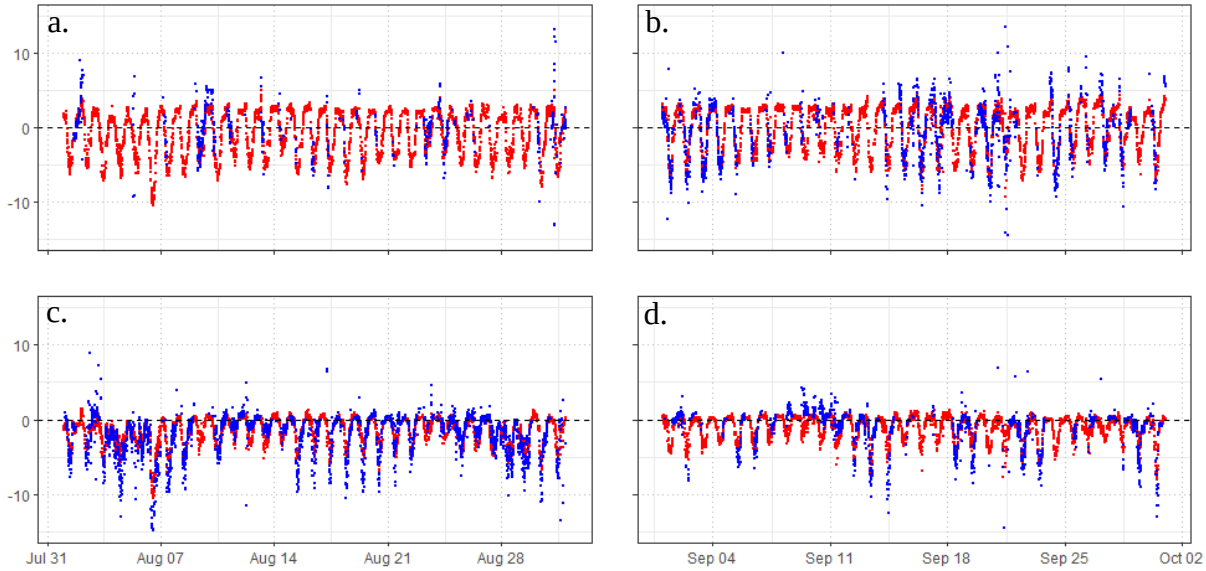

Figure 4. Atmospheric CO_2 fluxes (in µmol m^{-2} s^{-1}) measured by EC station (blue) compared to CO_2 fluxes predicted by the RF model (red) for the marsh (a, b) and mud habitat zones (c, d) during August (a, c) and September (b, d). These two months were chosen since they constituted two consecutive months in which each corresponding habitat was seen in majority by EC.

Concretely, to build the RF model, the data were divided into training and test sets, with 70% of the data used for training. The most powerful model was trained using following explanatory variables: Photosynthetically Active Radiation (PAR), relative humidity, air temperature, wind direction, air pressure, wind speed and water height. The Random Forest model was trained with 400 trees for each iteration, utilizing the "randomForest" v. 4.7 – 1.1 R package (Liaw and Wiener 2002). The model metrics indicated a Root Mean Square Error (RMSE) of 1.90, a coefficient of determination (R^2) of 0.62, and a bias of -0.016. Measured and predicted fluxes were compared graphically (Fig. 4; Annex. 2).

Then, with the random forest model fitted, missing values could be estimated from the values of the measured explanatory variables. Air pressure, wind direction and wind speed featured some few missing values (3%), so these latter were filled by a 6-hour moving average before using these variables to train the RF model.

Partial dependence plots (PDPs) were generated from the RF model for each variable used to train the model using the "pdp" v. 0.8.1 R package, and for both mudflat and marsh

zones (see result section, Fig. 6). PDPs permit to visualize the relationship between the explanatory variables and model predictions. For each value of the explanatory variable of interest, a grid of values covering its range was created. The model then predicted the response variable by setting the explanatory variable to each grid value and keeping all other variables at their initial observed values. This process was repeated over the entire grid, generating conditional predictions for each observation. These predictions were averaged for each fixed value of the explanatory variable, representing the average predicted response. By repeating this operation over the entire grid, we obtained a set of average predictions illustrating the marginal effect of the explanatory variable on the variable to be explained.

Additionally, the importance of each variable in the RF model construction was assessed to rank the influence of each explanatory variable. The metric "IncNodePurity" was used to quantify the contribution of each variable and to make the nodes of each decision tree the purest.

2.3. Water height measurements

During low tide, CO_2 fluxes measured by the station, i.e. the Net Ecosystem Exchange (NEE), reflects the net production of the benthic or terrestrial communities (NCP) from mudflat and marsh habitats. At high tide (rising and ebbing tides), it includes both contributions from the water column and the benthic interfaces, as well as horizontal exchanges with the ocean and terrestrial inputs (Polsenaere et al. 2012). To determine tidal dynamics at the site, a STPS probe (salinity, temperature, pressure sensor, NKE) was installed at the base of the EC station. This probe continuously measured water height, temperature, and salinity every 10 minutes. Water height measurements were corrected for atmospheric pressure. Higher atmospheric pressure exerts more force on the water surface, lowering the measured water height. The STPS probe was factory-calibrated at an atmospheric pressure of 1013hPa. To correct water heights, the difference between the real-time atmospheric pressure measured by the EC system and the reference pressure was subtracted from the recorded water heights. Additionally, water height measurements were considered null if the salinity measured by the sensor was below 2. The STPS probe measured water heights locally at a single point in the overall footprint of the EC station, introducing uncertainties related to the presence or absence of water spatially over the entire footprint. It was then essential to differentiate spring tides from neap tides, since during neap tides, water never reached the station even at high tide, whereas during spring tides water reached the station at high tide, with all the existing intermediate immersion situations in between.

2.4. CO_2 exchanges estimated at the water-atmosphere interface from autonomous pCO_2 measurements in the water column and gas exchange coefficient parametrization

CO_2 exchanges at the water-atmosphere interface were estimated using an autonomous water pCO_2 sensor (C-SenseTM; PME/Turner Designs) (Annex 3). The sensor measured dissolved CO_2 concentrations in water using a non-dispersive infrared (NDIR) detector. It was equipped with a semi-permeable membrane that allowed CO_2 to pass through while preventing water and contaminants from reaching the detector. This probe was resistant to biofouling. The measurement range was 0-2000 ppmv with an absolute accuracy of ± 60 ppmv. Sensors were installed during spring tide periods at least one week for all four seasons in the mud zone close to the EC station.

Raw pCO_2 data were corrected for total dissolved gas pressure (TDGP), which can influence measured pCO_2 values and improve the overall accuracy of the sensor. TDGP corresponds to the total pressure exhibited by all gases within the water column. When this pressure exceeded

the pressure at which the C-Sense probe was calibrated (1009 hPa), the output needed to be corrected as followed according to Mayen et al. (2023):

$$pCO2(cor.) = pCO2(mes.) \times 1009\ TDGP$$
$$TDGP = P(atm.) + P(sat.)$$
$$P(sat.) = \exp(13.7 - 5120\ T) \times 1013.2$$

With pCO_2(cor.) the corrected CO_2 partial pressure (ppmv); pCO_2(mes.) the water partial pressure of CO_2 measured (ppmv) with the C-Sense sensor; 1009 hPa is the atmospheric pressure on the day of calibration of the C-Sense sensor; TDGP is the total pressure of the gases dissolved in the water (hPa); P(atm.) is the atmospheric pressure (hPa); P(sat.) is the theoretical saturating vapor pressure (hPa; according to the Dupré-Rankine formula); T is the temperature of the water (in K). pCO_2 values associated with the gas transfer velocity and the CO_2 solubility coefficient in water allowed then calculating CO_2 fluxes at the air-water interface according to Polsenaere et al. (2013) and others:

$$FCO_2 = CO_2solulility \times k \times [pCO_2(water) - pCO_2(atm.)]$$

With FCO_2 the CO_2 fluxes at the water-atmosphere interface (mmol m^2 h^{-1}); $CO_2solulility$ the CO_2 solubility coefficient in water (mol Kg^{-1} atm^{-1}); k the CO_2 gas exchange coefficient (cm h^{-1}); $pCO_2(water)$ the corrected pCO_2 in water (ppmv) and $pCO_2(atm.)$ the atmospheric pCO_2 measured at the same time by the EC station. The CO_2 solubility coefficient depends on water temperature and salinity and was calculated according to Weiss (1974):

$$CO_2solubility = \exp(\alpha + \beta + \gamma)$$
$$\alpha = -60.2409 + 93.4717 \times 100\ T$$
$$\beta = 23.3585 \times \ln(T\ 100)$$
$$\gamma = S \times (0.023517 - 0.023656 \times T\ 100 + 0.0047036 \times (T\ 100)^2)$$

With T the water temperature (in K), S the water salinity and K the gas exchange coefficient parametrized for open coastal environments according to Wanninkhof (1992):

$$K660 = 0.31 \times (U10)\ 2 \times (Sc\ 660)\ -0.5$$
$$Sc = A - B \times T + C \times (T)\ 2 - D \times (T)\ 3$$

With $K660$ the exchange coefficient according Wanninkhof (1992) (in cm h^{-1}); $U10$ the wind speed at 10 meters (in m s^{-1}) calculated according Amoroko et Devries (1980); Sc describes both the water viscosity and the molecular diffusion of the subsurface layer; A = 2073.1, B = 125.62, C = 3.6276 and D = 0.043219 (Bade. 2009).

During year 2023, pCO_2 in the water column were recorded for Winter between 15/02 and 01/03, for Spring between 07/04 and 26/04, for summer between 26/06 and 10/07 and for Fall between 26/10 and 02/11.

2.5. Atmospheric CO_2 exchanges measured at the community scale at emersion by the benthic chamber methodology

At the sediment-atmosphere interface, CO_2 exchanges were measured using benthic chambers (Migné et al. 2002a). Theses chambers are made up of clear domes to measure the Net Community Production (NCP) and dark domes to measure the community respiration (CR).

The Gross Primary Production (GPP) was then calculate as GPP = NCP – CR. In the present study, domes measured 40 cm in diameter at the base and covered a surface area of 0.125 m², with a volume of 25L (Annex 3). The chambers have been deployed in all four seasons at both mudflat and marsh locations (Fig. 1) according to wind direction to be in the EC footprint and have the corresponding and simultaneous EC (NEE or NCP) values. On the marsh, the chambers were always deployed on *Halimione* because it is the halophyte plant community that is the most represented within the tidal marsh and seen by the EC station (Tab. 1). For saltmarsh chamber deployment, base plates were used to ensure chamber seal. The volume contained in the chamber then increased to 32L. The air circulates in the chamber in a closed circuit and passes through a gas analyzer (LiCor Li-830). Variations in CO_2 concentration (ppm) in the chamber were measured over a period of 30 minutes for each chamber. Each measurement was repeated three times at slightly different points.

From CO_2 concentrations, CO_2 fluxes were then calculated using the slope of CO_2 concentration (ppm) versus incubation time (s) obtained by linear regression. These values were then expressed in mmol m^2 h^{-1} using the following equation:

$$FCO2 = m.(\frac{V.3600}{Vm.S.1000})$$

With m the slope of CO_2 concentration (ppm/s). V the volume of the benthic chamber (L). Vm the molar volume of carbon (22.4 L/mol) and S the surface area of the chamber (m^2).

2.6. Statistical analysis

Statistical analysis was performed using R Studio (version 4.2.1). Data were classified into different marsh or mud habitat zones according to wind direction given by the EC station. Marsh zone was ranged between wind directions of 45° and 225° and mud zone was ranged above 225° and below 45° (Fig. 1 and 3). Daytime and night-time periods were identified using PAR values, daytime was defined as data measured at PAR > 10 µmol m^2 s^{-1}. Significant differences between groups were assessed using Kruskal-Wallis test, followed by Dunn's post-hoc test with Bonferroni correction. Relationships between CO_2 fluxes and other environmental parameters (PAR, air temperature, etc.) were explored using Spearman correlation coefficients and linear regression models, with separate analyses for daytime and nighttime periods. For all statistical analyses, a significance level (p-value) of 0.05 was set as the threshold of significance.

3. Results

3.1. Dynamics of atmospheric CO_2 exchanges and associated environmental parameters at global ecosystem scale

At the annual scale, 2023 was characterized by intense dry periods just before and at the end of the summer season (Fig. 5b); May, June and September were the driest months with average relative humidity (RH) values of 72, 74 and 75%, respectively. In contrast, January and December were the wettest months (86 and 88%). In addition, June and September were the warmest months (i.e. 21°C in average), when January and February were the coldest months with monthly average values of 6.9 and 6.4°C, respectively (Fig. 5b). In particular, the warm and dry period observed during the end of spring and early summer was associated with daily atmospheric CO_2 fluxes measured by EC shifting from negative to positive values (Fig. 5a). Fluxes shifted from an average of -1.98 µmol m^{-2} s^{-1} the 23/05 to 2.13 µmol m^{-2} s^{-1} the 28/05. This period was also the brightest of the year, with Photosynthetically Active Radiation (PAR)

values above 2400 µmol m^{-2} s^{-1} at mid-May. Throughout the year, the brightest months corresponded to spring and summer seasons and the lowest light months occurred in fall and winter (Fig. 5c).

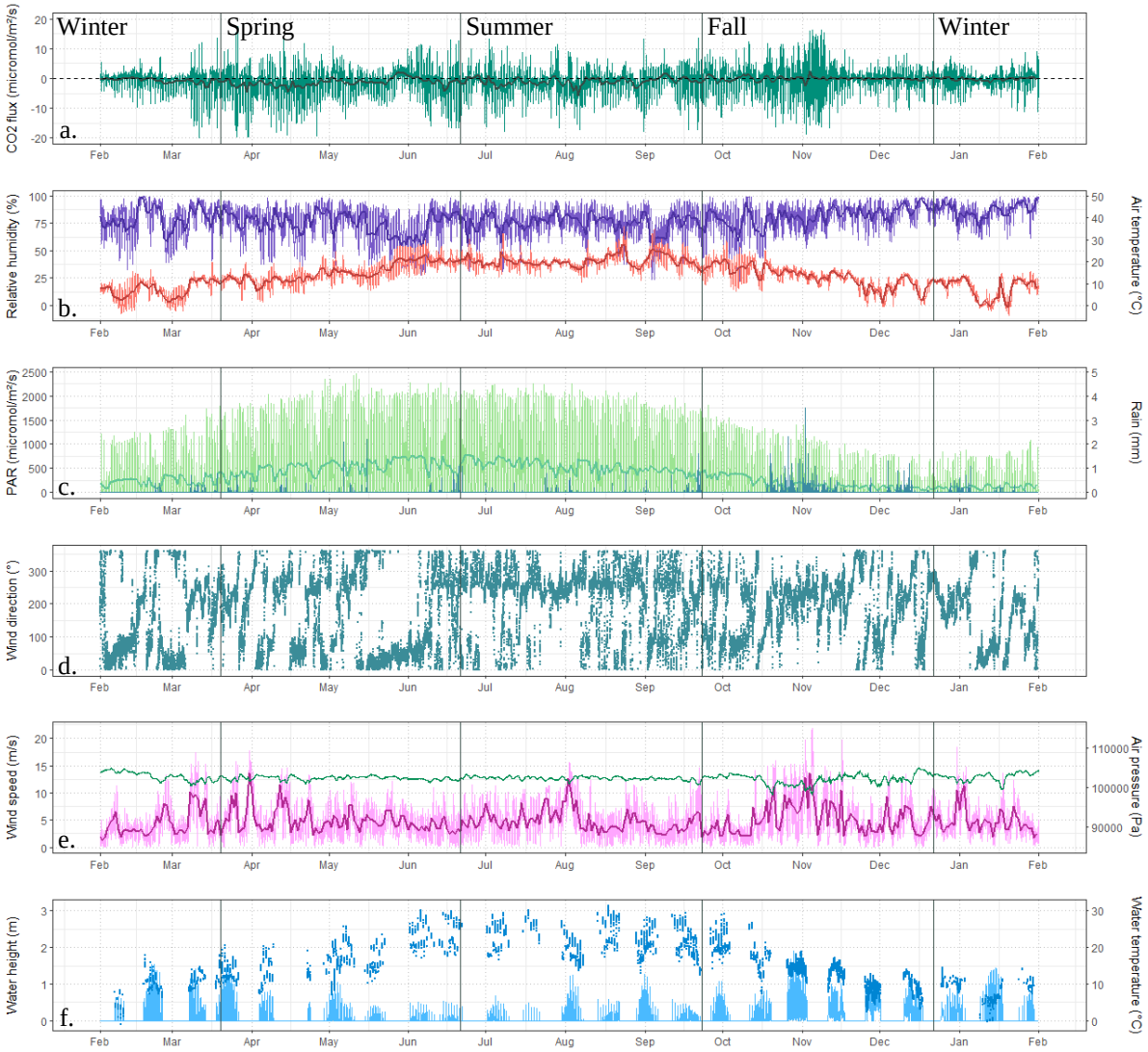

Figure 5. Eddy Covariance time series from 01 February 2023 to 31 January 2024 of (a.) atmospheric CO_2 exchanges, (b.) relative humidity (violet) and air temperature (red), (c.) Photosynthetically Active Radiation (PAR, light green) and rain (blue), (d.) wind direction, (e.) wind speed (pink) and air pressure (green), and (f.) water height (light blue) and water temperature (dark blue). For CO_2 fluxes, relative humidity, air temperature, PAR and wind speed, the continuous line represents the daily average obtained from the 10 min. values.

At the study site, wind directions measured by the EC station, allowed seeing the different habitat compositions in the corresponding EC footprints and their potential relationships with measured turbulent fluxes (Tab. 1; Fig. 3; and M&M section). Atmospheric CO_2 fluxes came from the mudflat zone when wind directions were above 220° and below 60° (Fig. 3). Outside this wind direction sector, measured EC fluxes corresponded to a habitat mosaic with salt marsh (halophilic plants) and mudflat (microphytobenthic communities) zones (referred to the "marsh" zone in the following) in different proportions included in the EC footprints (Tab. 1; Fig. 3). Monthly mean EC footprints ranged from a minimum surface of 13 ha in August to a maximum surface of 110 ha in April; the yearly mean EC footprint surface was estimated at 86

ha (Tab. 1; Fig. 3). Over the year, 38% of wind directions came from the marsh zone and 62% from the mudflat zone. Specifically, during the late May dry period, wind directions came exclusively from the mudflat when in summer, winds were predominantly from the west and rarely from the east directions (Fig. 5d). Thus, the mudflat represented about 92% of the western sectors (WSW-WNW) and about 23% of mud and 77% of marsh composed the eastern sectors (ENE-ESE) of the yearly mean footprint (Fig. 3). Consequently, the mudflat zone generally dominated the footprint, with the highest recorded surface contribution occurring in the winter and spring seasons (i.e. in April, 77.2 ha) and the lowest one during summer (i.e. in July 6.0 ha). However, in summer, the very low mudflat area contribution in the footprint was not offset by a higher marsh halophytic plant *Halimione* contribution for which the maximum extends rather occurred in autumn/winter (i.e. in January 25.8 ha and in October 25.0 ha). Other types of vegetation, such as *Puccinelia*, *Agropyron*, *Aster*, *Salicornia* and *Spartina* also contributed with generally lower and more stable surfaces except in summer.

From mid-October to mid-November of the year 2023, stormy weather periods occurred and were characterized by very important wind speeds (reaching 22 m s^{-1} the 04/11/2023), very low atmospheric pressure values (dropping to 980 hPa, 20/10/2023) and heavy rain events reaching 3,5 mm the 01/11/2023 for instance (Fig 5c; Fig. 5e). These weather conditions resulted in a high variability of measured atmospheric EC CO_2 fluxes (Fig. 5a). During winter months, atmospheric CO_2 fluxes were relatively low, fluctuating around zero and a mean winter value of -0.72 ± 2.49 µmol m^{-2} s^{-1}. In spring and summer, the variability of CO_2 fluxes increased, with more frequent and pronounced negative values but also some positive value peaks. Seasonal mean fluxes values reached -1.18 ± 3.38 µmol m^{-2} s^{-1} in Spring and -1.04 ± 3.11 µmol m^{-2} s^{-1} in summer. The maximum negative 10-minute EC flux value (-27.6 µmol m^{-2} s^{-1}) was measured the 13/04/2023 when the maximum positive one (17.6 µmol m^{-2} s^{-1}) was measured the 26/03/2023. After this mid-fall high flux variability period, daily averaged fluxes dropped back to values near zero and a lower fall flux variability period was observed with a seasonal mean value of -0.08 ± 2.43 µmol m^{-2} s^{-1}. Globally, over the full year, the negative averaged flux value (-0.75 ± 2.92 µmol m^{-2} s^{-1}) measured by the EC station indicated a CO_2 sink behavior of the whole studied ecosystem zone (mudflat/marsh). Over this year of EC measurements, oceanic waters reached the EC station only 17% of time. The mudflat was covered by water, with water heights at the station exceeding 0.25 m, only 9.7% of the year. The maximum water height recorded at the station was 1.92 m.

3.2. Atmospheric CO_2 flux dynamics and environmental controls according to habitat composition at the studied site

At the global EC footprint scale (i.e. whole ecosystem with mudflat and marsh zones), PAR had a positive effect (in absolute values) on atmospheric CO_2 fluxes, and this effect was stronger over mosaic marsh than mud habitats (Fig 6a). This difference was even more significant for the other variables influencing measured EC CO_2 fluxes. For relative humidity, air temperature and wind speed variables, patterns seemed similar between both habitats though more negative fluxes were predicted for mudflat in comparison with mosaic marsh habitats (Fig. 6b; Fig. 6c; Fig. 6e). At a relative humidity threshold close to 45%, on the marsh zone, flux prediction shifted from a decrease to an increase (less negative flux values) (Fig. 6b). For air temperature thresholds of about 9°C for the mud and 14°C for mosaic marsh zones, fluxes greatly increased toward fewer negative values (Fig. 6c). At wind speed thresholds of 9 m s^{-1} for marsh and 12 m s^{-1} for mud zones, flux prediction shifted from important decrease to increase values (Fig. 6e). An increase of atmospheric pressure values reduced negative predicted fluxes for the marsh zone and to the contrary, increased negative predicted fluxes for the mudflat zone (Fig. 6d). The effect of water heights seemed to stabilize flux values as soon

as threshold values of 0.5m for the marsh and 0.15m for the mudflat were reached. From water height threshold of 1m, atmospheric CO_2 fluxes greatly decreased to more negative values for both zones before remaining constant again from 1.25m of water height (Fig. 6f).

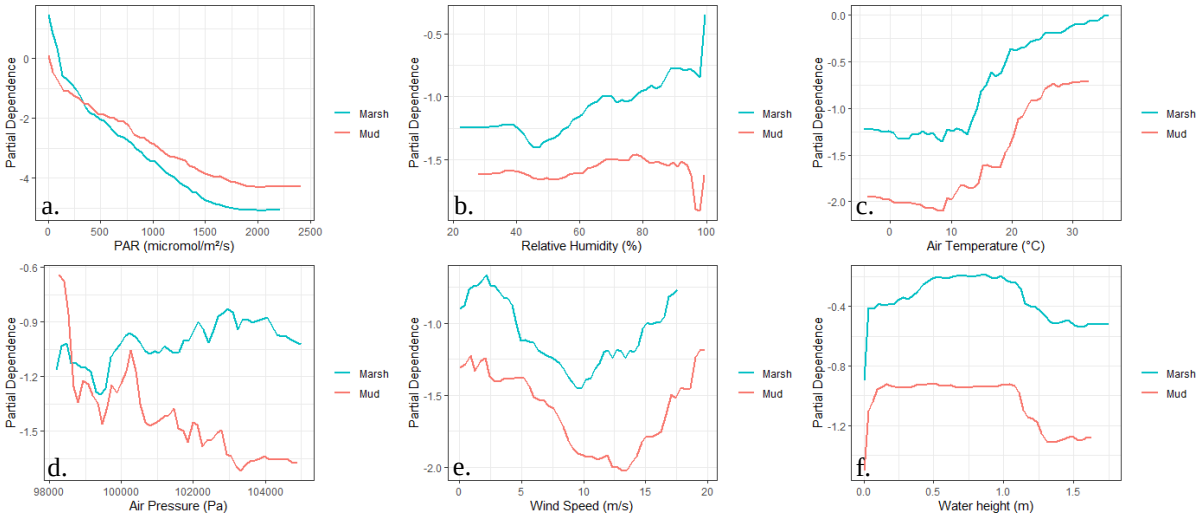

Figure 6. Plots of partial dependence of CO_2 fluxes on different environmental parameters for "mud" (in red) and "marsh" (in blue) data. These Partial Dependence Plots (PDPs) were built using the random forest model (see M&M section).

These different variables did not have the same importance in the construction of the RF model. PAR (89308) was the most important variable, followed by wind direction (32764), air temperature (Ta) (31556) and relative humidity (RH) (27831). Wind speed (26106) and atmospheric pressure (24704) contributed to the model to a lesser extent. Finally, Hw (7096) was identified as the least important variable in the construction of the model (see M&M section for more details).

The importance of PAR in predicting CO_2 fluxes was seen in the difference between daytime and night-time measured fluxes. On the mud zone, annual fluxes were divided into important daytime negatives fluxes (-2.37 ± 2.91 µmol m^{-2} s^{-1}) and weaker night-time positive fluxes (0.03 ± 1.37 µmol m^{-2} s^{-1}). On the marsh, annual fluxes were divided into close daytime and nighttime fluxes in absolute value, -1.94 ± 3.40 µmol m^{-2} s^{-1} and 1.47 ± 1.69 µmol m^{-2} s^{-1}, respectively. Mean CO_2 fluxes at daytime coming from the WSW footprint sector were much more negative than flux values from the other sectors of the mudflat zone (-2.92 ± 3.13 µmol m^{-2} s^{-1}). For the marsh zone, daytime and nighttime mean fluxes from the eastern sectors were higher than flux values from the southern sectors (Fig. 7). Comparing marsh and mud fluxes at daytime, ENE-NNW, ENE-WNW, SSE-NNE and SSW-WNW sector flux values were not significantly different from each other (Kruskal-Wallis and Dunn tests: p = 0.07; p = 0.50; p= 0.43; p= 0.13 respectively, Fig. 7). The annual mean flux values were -1.27 ± 2.62 and -0.12 ± 3.13 µmol m^{-2} s^{-1} for the mud and marsh zones, respectively. For the ENE and SSE marsh's sectors, mean annual fluxes were close to 0, i.e. -0.04 ± 3.22 µmol m^{-2} s^{-1} and -0.18 ± 2.55 µmol m^{-2} s^{-1}, respectively. For the ESE sector, an annual average value of 0.43 ± 3.27 µmol m^{-2} s^{-1} was measured, meaning positive flux values were higher than negative flux values. For the SSW sector, with an annual mean flux value of -0.52 ± 3.19 µmol m^{-2} s^{-1}, the opposite trend was found. Finally, for mud sectors, mean annual flux values were more negative, meaning positive values were much weaker than negative flux values, though to a lesser extent for the NNE sector (Tab. 2).

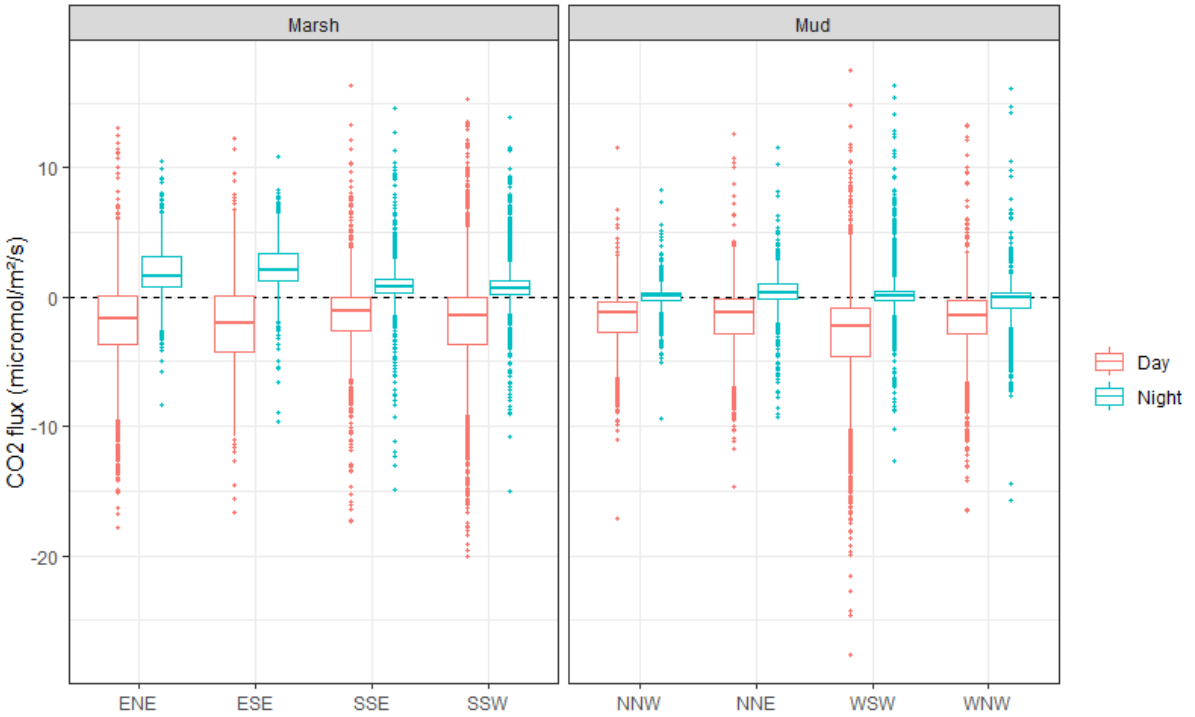

Figure 7. EC CO_2 flux distribution according to daytime (red), night-time (blue) periods and the different wind sectors with associated habitat zones (Mud and Marsh, see M&M section).

Table 2. Mean CO_2 flux values with standard deviation (in µmol m^{-2} s^{-1}) for each wind sector.

Marsh				Mud			
ENE	**ESE**	**SSE**	**SSW**	**NNW**	**NNE**	**WSW**	**WNW**
-0.04 ± 3.22	0.43 ± 3.27	-0.18 ± 2.55	-0.52 ± 3.19	-0.72 ± 1.74	-0.59 ± 2.18	-1.86 ± 3.03	-0.96 ± 2.14

3.3. Metabolic fluxes at emersion

In the mudflat zone, Net Community Production (NCP) measured by benthic chambers was comprised between -0.74 ± 0.36 and -4.23 ± 0.86 µmol m^{-2} s^{-1}, respectively in fall and summer. In the marsh, more negative NCP values were found in fall (-4.59 ± 1.43 µmol m^{-2} s^{-1}, Tab. 3). In the mudflat, unlike the marsh, Community Respiration was difficult to measured. In summer, mudflat benthic chamber measurements revealed weak CR values, with a mean value of 1.31 ± 0.38 µmol m^{-2} s^{-1}. In marsh, CR values were, in average higher, reaching 8.36 µmol m^{-2} s^{-1} in summer for instance (Tab. 3).

Table 3. NCP and CR measurements and GPP calculated (in µmol m^{-2} s^{-1}) from benthic chambers measurements at low tide (emersion). Each value is the average of the tree replicates.

	MUD			MARSH		
	NCP	**CR**	**GPP**	**NCP**	**CR**	**GPP**
Winter	-1.34 ± 0.85	0.14	-0.57	-0.31 ± 0.06	3.55 ± 0.84	-3.87 ± 0.91
Spring	-1.56 ± 0.47	/	/	-2.51 ± 1.65	6.67 ± 1.27	-9.18 ± 0.87
Summer	-4.23 ± 0.86	1.31 ± 0.38	-5.53 ± 1.22	-0.88	8.36	-10.56
Fall	-0.74 ± 0.36	/	/	-4.59 ± 1.43	6.13 ± 1.32	-10.72 ± 1.18

At emersion and in absence of water within the footprint, EC fluxes represents the NCP during daytime and the CR during night-time. On the emerged mud zone during daytime, 86%

of EC flux data were negative when at night-time, 57% were positive. During daytime, fluxes were more correlated with PAR (-0.54) than with air temperature (-0.04) and relative humidity (0.09). During night-time, CO_2 fluxes were more correlated with air temperature (0.12) than relative humidity (-0.02). All these correlations were significant. PAR explained 22% of the total flux variability during the day and air temperature explained only 1% of the total flux variability during the night (Fig. 8). Night-time fluxes included a wide range of both positive and negative outliers (Fig. 8b). During the day, a clustering of points slightly above but close to zero was observed for PAR values above 1500 µmol m^{-2} s^{-1} (Fig. 8a). This clustering was no longer observable when the data corresponding to hot, dry weather were removed (late May and early September) (Annex. 4). Calculating the NEE vs PAR ratio allowed identifying periods when biogeochemical processes were potentially active (Fig. 9). Monthly, absolute slope values from EC flux versus PAR linear regressions, ranged from 0.0006 to 0.0037 µmol m^{-2} s^{-1} per µmol m^{-2} s^{-1} of PAR, with the most important slopes observed in May (0.0024 µmol m^{-2} s^{-1}) and September (0.0037 µmol m^{-2} s^{-1}). From October to January, slopes were relatively weak, ranging from 0.0006 (December) to 0.0014 (October). All of the correlations were significant except in December (p = 0.058)

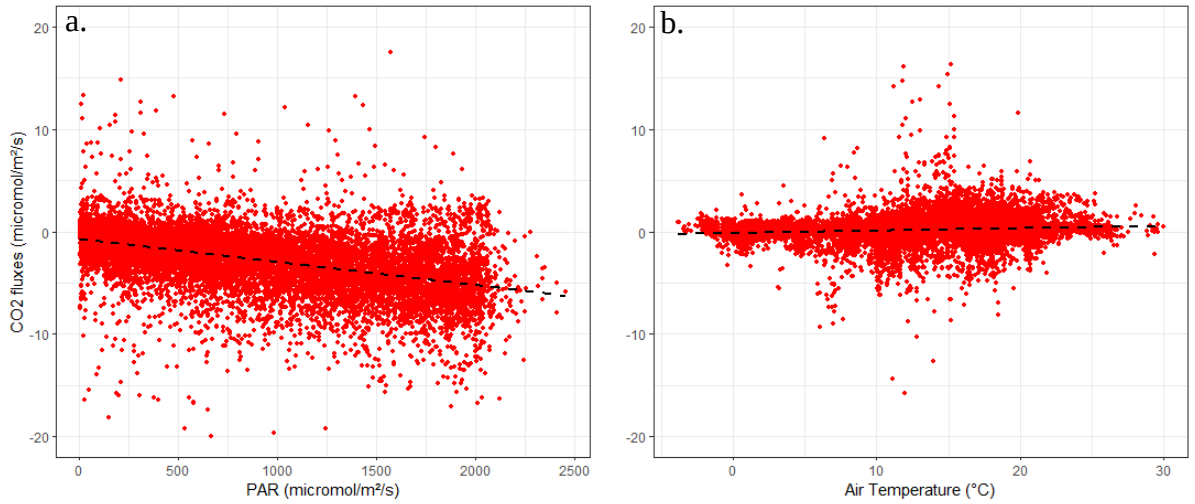

Figure 8. Daytime EC fluxes measured over the mudflat zone according to PAR values (a) and night-time EC fluxes according to air temperature values (b). Dotted black line represents the linear regression.

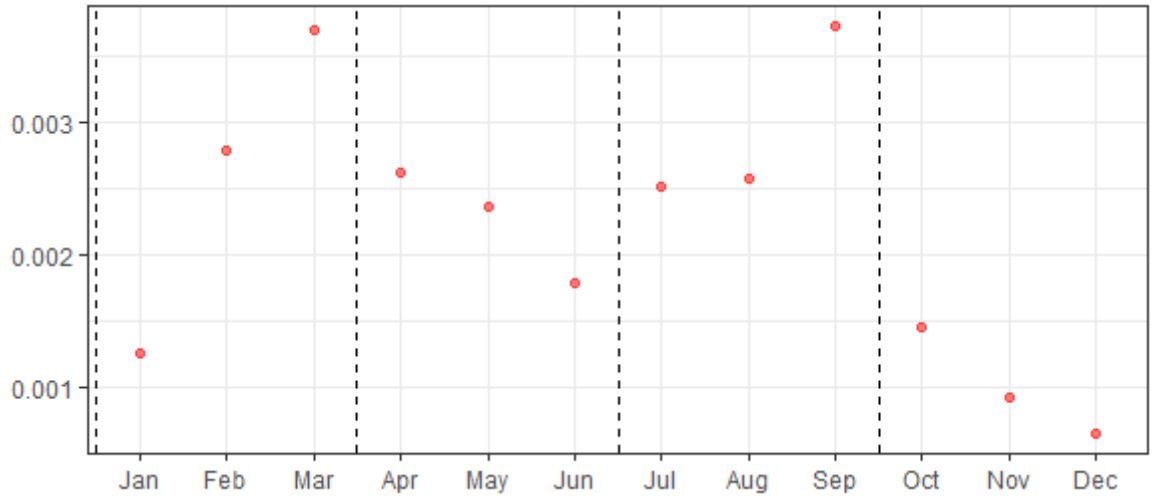

Figure 9. Linear regression absolute slope values of CO_2 fluxes (in µmol m^{-2} s^{-1}) according to PAR values (in µmol m^{-2} s^{-1}) for each month.

3.4. Water influence on atmospheric CO_2 flux dynamic

Over the year, the EC station was tidally immerged at high tide at least once per day for 190 days. During daytime, CO_2 fluxes were widely variable depending on the tidal period, with the most negative values generally measured during spring low tides except for February and April. At daytime spring low tides, monthly average fluxes ranged from -1.07 ± 1.53 µmol m^{-2} s^{-1} (January) to -4.42 ± 4.20 µmol m^{-2} s^{-1} (March). From May to November, EC fluxes measured at high tide and fluxes measured at neap low tide were on average very close (Fig. 10a). High tide fluxes were for each month, on average, near zero except for July (-1.76 ± 1.45 µmol m^{-2} s^{-1}) and August (-2.21 ± 2.07 µmol m^{-2} s^{-1}) months that showed slightly more negative flux values. During night-time, fluxes measured at high tide during July were also greatly negative compared to the other months. Globally, during night-time, CO_2 flux variability between the different tide periods was reduced in comparison with daytime averaged flux values mostly close to zero. However, in January and July, night-time CO_2 fluxes at high tide were on average slightly more negative with flux values of -0.82 ± 1.67 µmol m^{-2} s^{-1} and -2.30 ± 1.45 µmol m^{-2} s^{-1}, respectively. These 10 min. flux values were even exclusively negative during July. In June, night-time CO_2 fluxes measured at high tide were exclusively positive (-1.27 ± 0.38 µmol m^{-2} s^{-1}) (Fig. 10b).

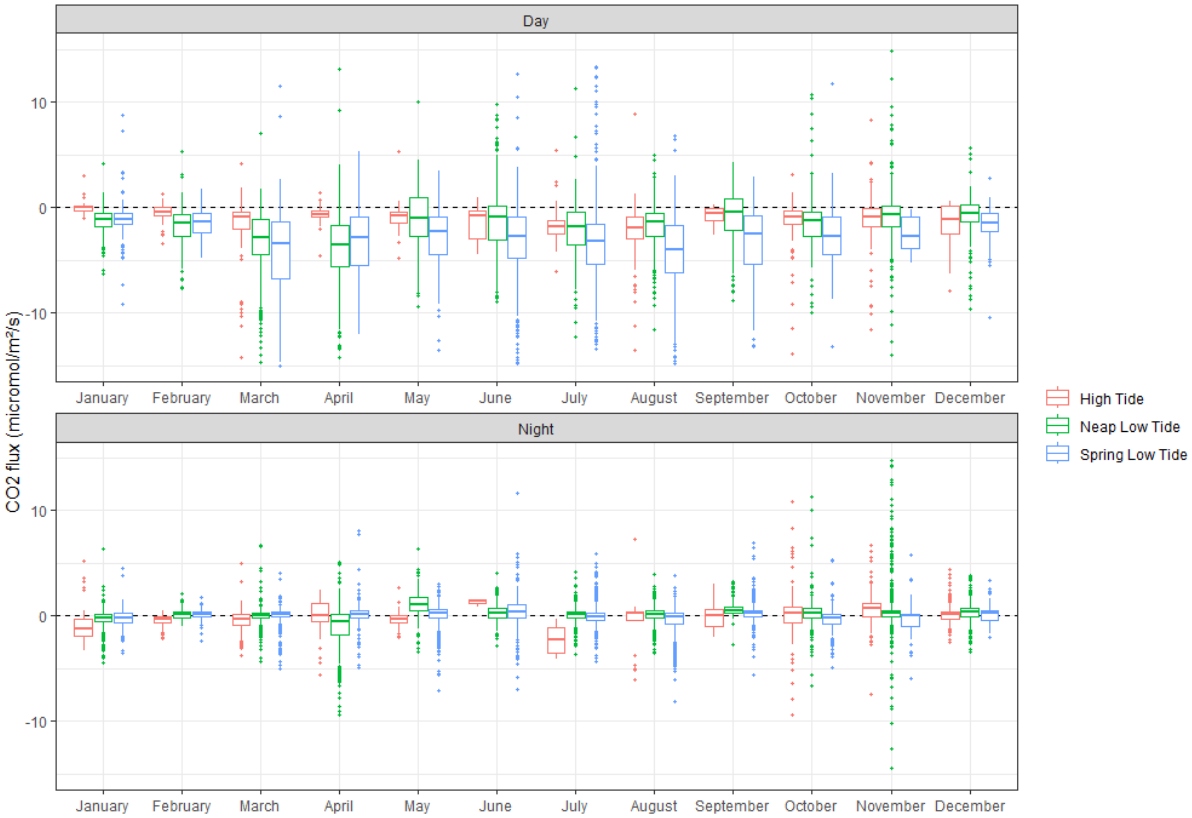

Figure 10. Monthly CO_2 flux distribution at immersion for day and night periods. High Tide represents fluxes measured when the water heights at the base of the station were above 0.25m.

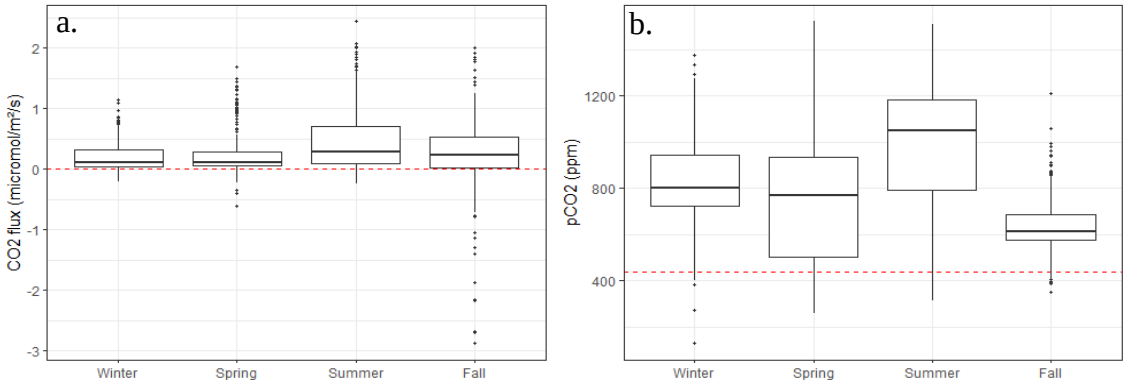

Figure 11. Water-air CO_2 fluxes (a) calculated from water pCO_2 measurements (b) (see M&M section d.). Red lines represent the limit between negative and positive fluxes (a) and the average atmospheric CO_2 concentration (b).

From water pCO_2 measurements, calculated water-air fluxes at high tide in winter and spring showed relatively low and stable CO_2 flux values, while summer and autumn months showed higher and more variable fluxes (Fig. 11a). In autumn, fluxes were not exclusively positive (i.e. -2.9 µmol m^{-2} s^{-1}), these negative fluxes always occurred just at the beginning of spring high tide. For all seasons, positive water-air CO_2 flux values resulted from over-saturated waters (water pCO_2 above the corresponding air equilibrium pCO_2) (Fig. 11b). Summer season was particularly characterized by CO_2 over-saturated waters with on average 980 ± 265 ppm. In contrast, fall season showed the weaker over-saturated waters (635 ± 119 ppm) due to numerous values below the mean atmospheric CO_2 concentration, specifically at the very beginning of each flooding tide.

3.5. Carbon budget of the mudflat zone

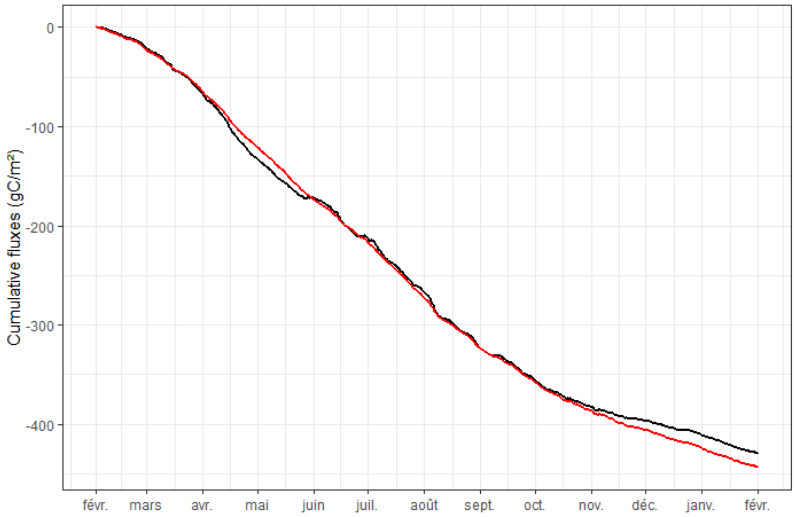

Figure 12. Yearly cumulative CO_2 fluxes for the mudflat zone i) computed from the measured and gap-filled 10 min. EC flux values (in black) and ii) fully computed from the RF model predicted fluxes (in red). Fluxes were predicted using a constant wind direction of 315° to estimate fluxes values in 'mud' conditions.

For the mudflat zone seen in the EC footprint above 225° and below 45°, the annual cumulated measured and gap-filled fluxes reached a value of -430 gC m^{-2} yr^{-1}. Throughout the year, a strong increase in the cumulative CO_2 uptake occurred until late May. Between late May and early June, cumulated CO_2 uptake slightly decreased (Figure 12). The cumulative CO_2 uptake increased again to the mid-October period before reducing until the end of the year. Predicted fluxes presented a similar but smoother trend, without reproducing all the variability observed in measured gap-filled cumulated EC fluxes (Figure 12). Predicted cumulated fluxes reached a value of -444 gC m^{-2} yr^{-1}. During April and May with predicted fluxes, CO_2 uptake was under-estimated whereas from mid-October CO_2 uptake was over-estimated.

4. Discussion

4.1. Methodological considerations for atmospheric CO_2 exchanges measurements over an intertidal marsh system

In the present study, different methods were used to assess large- and small-scale variability in atmospheric CO_2 fluxes over tidal marsh system as the temperate Aiguillon bay. The EC station allowed large-scale flux measurements over an area of approximately 86 hectares in average. Generally, EC deployments over terrestrial or coastal systems are done over rather homogeneous habitat zones (i.e. salt marsh in Mayen et al. 2024; mudflat in Polsenaere et al. 2012). In the present study, the area surrounding the EC station was not uniform and included both marsh and mudflat areas. Both habitats also presented heterogeneity according to halophytic plants on the marsh or MPB distribution on the mudflat along environmental controls**.** One of the objectives of the study was to reveal and associate the dynamics of each habitat with corresponding measured CO_2 fluxes by the EC station deployed right at the edge of both the mudflat and marsh habitat zones. However, logistical constraints (i.e. too low water heights due to strong anticyclonic conditions) required setting up the EC tower around 100 meters downstream from the marsh on the mudflat. Consequently, it was complicated to strictly isolate fluxes coming exclusively from halophytic vegetation, as the measurement footprint towards the marsh zone included a mosaic of the mud and marsh areas in different proportions as described in this study, and particularly close to the station. However, during daytime, the EC station generally measured fluxes coming from areas close to the station, unlike at night, due to differences in atmospheric stability. Indeed, during night-time, atmosphere often becomes more stable as the ground gets colder and creates a temperature inversion, where warmer air is above the cooler air that is near the surface of the ground. This stability reduces turbulence, allowing the air to move horizontally for longer distances before being detected by the sensors. Conversely, during daytime, air temperatures rise and create a more turbulent and unstable atmosphere, leading to more localized and vertical mixing, so that fluxes measured come from areas closer to the station (Vesala et al. 2008; Burba 2013). Footprint calculations separating daytime and night-time periods were done and associated footprints are presented in Annex 5 along Fig. 3 presenting the averaged footprint including both day and night-time periods. During the day, on average over the year 2023, the salt marsh was only seen within the footprint isocontour at 80% when, in the direction of the marsh, the mudflat contributed almost at 80% of fluxes measured by the EC station. Then, the lack of ability to isolate distinctly fluxes from marsh habitat complicated the interpretation of CO_2 dynamics specific to halophytic vegetation. In addition to the actual station deployed at the marsh - mudflat edge, another station could be added in the future within the marsh itself to measure exchanges within this single zone taking into account the heterogeneity that also exist within too.

The heterogeneous environment of the tidal marsh of the bay of Aiguillon was also behind a significant microtopographic variability. This heterogeneity was further influenced by a high

rate of sedimentation, leading to dynamic changes in soil morphology (Amann et al. 2023). At the base of the EC station, a STPS probe continuously measured water heights. Unlike EC measurements, which give high temporal and spatial resolution fluxes, the STPS probe provided water height data at a single point. On the site, the flooding tide is influenced by a network of canals that are filled and overflowed in a non-linear way, inversely at ebbing tide and differently according to spring and neap tide periods. Given this water mass movement complexity at the studied marsh system, these single-point measurements could have introduced uncertainties. For example, during a rising high tide, water could already cover parts of the footprint while the sensor was still recording a water height of zero. Conversely, when the tide retreated, water could remain in some areas of the footprint even though the sensor indicated that there was no water. This difference made it difficult to clearly identify water-covered versus dry zones within the footprint at certain periods, which was crucial since the presence or absence of water has a strong influence on the dynamics of CO_2 fluxes at the site as described in the present study and elsewhere. As a result, interpretation of our flux measurements became sometimes difficult due to the potential mismatch between actual flooding patterns and sensor readings. This problem also extended to flux modelling efforts that integrated water height data; a less accurate flood data could lead to less confident model predictions. Thus, spatial and temporal imprecisions of water immersion data could affect the interpretation of observed fluxes and the robustness of flux modelling. To reduce the uncertainties associated with point measurements of water levels, it would be useful to incorporate water level models developed at the LIENSs (Xavier Bertin researches and Loes Le Goff Le Gourrierec PhD work on the Aiguillon bay). These models, combined with digital elevation models (DEMs) that consider site elevation and vegetation height, could provide a better understanding of flooding and drying patterns spatially in the EC footprint. This would improve the accuracy of measurements and modelling of CO_2 fluxes, particularly for understanding the dynamics of NEE, NCP and CR within different habitats according to tidal rhythm and immersion versus emersion periods. In addition, the installation of several STPS sensors in the study area would also improve the accuracy of the water cover data, which would help to refine the interpretation of fluxes and improve the reliability of flux models. Already, during the summer of 2024, three additional STPS probes have been strategically installed to better understand the irrigation of the marsh.

The ability of the EC method to measure CO_2 fluxes at very high spatial and temporal frequency represents a key advantage in comparison with other methods. For instance, benthic chambers (BC) as deployed here are complementary even if temporally and spatially limited to small localized areas, generally at the scale of single communities. While benthic chambers provide accurate, site-specific measurement values, their spatial coverage is extremely limited and often captures only a small fraction of the heterogeneity present in ecosystems such as our study site (Migné et al. 2002a; Ouisse et al. 2011; Spilmont et al. 2006). In addition, BC measurements are generally taken over short periods, making it difficult to capture long-term processes such as respiration, particularly in dynamic mudflats. In our case, these limitations were important. Chamber deployments at night could be carried out to better capture the true in situ respiration activity (Lee et al. 2011).

4.2. Temporal variability in atmospheric CO_2 exchanges over the mudflat part of the Aiguillon Bay tidal marsh system

The Bay of Aiguillon mudflat zone is covered by microphytobenthos (MPB) communities, essentially composed of diatoms, as commonly observed in intertidal ecosystems (MacIntyre et al. 1996; Savelli et al. 2018; Méléder et al. 2020). These photosynthetic microorganisms use light energy to convert CO_2 into organic matter, a process that significantly contributes to CO_2

uptake when light availability is sufficient (Cahoon 1999). Compared with previous studies, this study also confirms a net CO_2 uptake from the mudflat during productive periods of high photosynthetic activity (Migné et al. 2002). At emersion, EC and BC techniques measured, respectively, a daytime CO_2 uptake up to -2.93 ± 2.98 and -4.23 ± 0.86 µmol m^{-2} s^{-1} in Summer. However, during warm and dry weather conditions, the relationship between light availability and EC CO_2 flux was weaker. This could be due to photoinhibition or thermal stress, which reduced the photosynthesis activity (Hancke and Glud 2004; Polsenaere et al. 2012).

Must of night-time fluxes were positive, indicating that mudflat acted predominantly as a source of CO_2 during these periods. A part of this source could be explained by the respiration of MPB and benthic macrofauna which feed on MPB (Polsenaere et al. 2012). However, given the very slight effect of respiration on night-time flux variations, macrofauna was probably not too abundant on the studied mudflat as observed elsewhere (Migné et al. 2009). Moreover, during night-time, despite the absence of light, the mudflat ecosystem occasionally acted as a sink of atmospheric CO_2 as shown by some negative flux values measured over the full year. For instance, night-time negative EC fluxes reached -9.33 µmol m^{-2} s^{-1} in April 21, 2023 at 4:30 am and -14.42 µmol m^{-2} s^{-1} in November 6 at 9:20 pm. These night-time CO_2 uptakes were probably due to biological processes (other than photosynthesis) and physico-chemical processes linked to CO_2 solubility according to water temperatures. For example, the Curé channel running through the mudflat and seen in the EC footprint, with waters generally CO_2 over-saturated, could become undersaturated at certain period. Water pCO_2 measurements done in Coignot et al. (2020) showed a slight undersaturation (426 ppm) of the channel in autumn 2018. The CO_2 sink behavior of the Curé channel waters could then drive the overall CO_2 sink of the mudflat zone measured by the EC station especially with its associated low respiration rates. Moreover, as explained in this study, water bodies could remain in the EC footprint at low tide (i.e. water trapped in small basins at ebbing tide due to microheterogeneity or oceanic water presence remaining at spring tide). These water bodies could sometimes be undersaturated due to carbonate dissolution leading to an overall CO_2 sink status of the mudflat zone (negative EC fluxes) even at night as observed over other tidal bay systems nearby (Polsenaere et al. 2012; Polsenaere et al. 2023; Rigaud et al. 2018).

4.3. Habitat heterogeneity and influence on atmospheric CO_2 fluxes over the salt marsh system

BC measurements on *Halimione* revealed significant seasonal variations in NCP and CR, similarly to BC measurements performed on *Spartina* in spring/summer 2023 at the same studied site (Amiar 2023). For both communities, primary production was higher in spring than in summer. Conversely, CR rates were higher in summer than in spring. In summer, *Spartina* and *Halimione* CR were really close, -0.84 and -0.88 µmol m^{-2} s^{-1} respectively. These results suggested that both communities similarly reacted to seasonal environmental changes this year. Only *Spartina* respiration rates were lower than those of *Halimione* in each season, i.e. in spring with 3.04 ± 0.79 µmol m^{-2} s^{-1} for *Spartina* and 6.67 ± 1.27 µmol m^{-2} s^{-1} for *Halimione*; it endorses the relatively short growing period of this perennial *Spartina* species and a potentially lower influence on carbon marsh metabolism in comparison with *Halimione* especially during these non-productive seasons as shown by Mayen et al. (2024) in another salt marsh nearby.

The western and northern sectors seen in the EC footprint, composed mainly of the homogeneous mudflat part with only minor influences from the Curé channel, were relatively straightforward to approach. In contrast, as the year progressed from winter to spring/summer seasons, the mud part between the marsh and the EC station was increasingly colonized by *Spartina*, further complicating CO_2 flux analysis. *Spartina* species are known for their high CO_2 uptake due to their high photosynthetic capacity and ability to grow in intertidal environments

(Mendelssohn et Morris 2002). In the eastern and southern sectors, the area very close to the station which initially consisted mainly of mudflat areas, became more heterogeneous, with patches of *Spartina* that could influence the EC CO_2 flux dynamics in these sectors. During daytime, EC station measured a higher average CO_2 uptake in the WSW sector compared to the others. This higher uptake was probably due to the colonization of *Spartina* in this zone, which could enhance photosynthetic activity and therefore the CO_2 sink. *Spartina* colonization is a well-documented process in intertidal zones, where these plants can significantly alter both physical landscape and biogeochemical processes, including carbon dynamics (Callaway et Josselyn 1992; Li et al. 2009).

4.4. Tidal influence on atmospheric CO_2 exchanges on the mudflat zone

In 2023, EC measurements from the mudflat zone revealed mean daytime fluxes of -2.45 ± 2.92 µmol m^{-2} s^{-1} and night-time fluxes of 0.04 ± 1.34 µmol m^{-2} s^{-1}. These results indicated that, on average, the mudflat acted as a net sink for CO_2 during the day, but as a lesser source at night. Considering fluxes over immersion periods only, diurnal CO_2 fluxes decreased to -1.45 ± 2.09 µmol m^{-2} s^{-1}, while nocturnal fluxes shifted to -0.02 ± 1.53 µmol m^{-2} s^{-1}. This dynamic suggested a reduction in biological activity on the mudflat in response to sediment immersion by coastal waters, but could also reveal the occurrence of other processes (biological, physical or chemical) at the water-atmosphere interface. Firstly, atmospheric CO_2 uptake at immersion are reduced by the physical barrier created by the water column, which limits the direct exchange of gas between sediments and the atmosphere (Kathilankal et al. 2008; Polsenaere et al. 2012; J. Mayen et al. 2024). Secondly, flooding also affects the photosynthetic activity of microphytobenthos and associated atmospheric fluxes decreasing light availability in the water column. What's more, these organisms tend to migrate into the sediment to avoid resuspension in the water column (MacIntyre et al.1996) that can be particularly important (i.e. 25%) in these systems as observed by Savelli et al. (2018) in a nearby mudflat.

As described in the present study, over the mudflat zone at low tide, it was necessary to analyze CO_2 flux dynamics according to tidal periods, i.e. spring and neap tides. Mean fluxes were more negative during low spring tides than during neap tides, with diurnal fluxes of -3.21 ± 3.08 versus -1.94 ± 2.72 µmol m^{-2} s^{-1}, respectively. This might suggest that the primary production of the mudflat could have been greater when the latter was wetted a few hours earlier. During night-time, mean fluxes were slightly positive for neap low tides (0.11 ± 1.43 µmol m^{-2} s^{-1}), while they were almost neutral or even negative for spring low tide periods (-0.05 ± 1.14 µmol m^{-2} s^{-1}) with mudflat sediments more water saturated too due to recent immersions. Due to the absence of light, these measured uptakes could not be attributed to the MPB photosynthesis activity but could rather be due to CO_2 undersaturated water body presence in the EC footprint as observed at the studied site (see section b. above). In contrast, at low tide during neap tide periods, the mudflat remained exposed and dry for longer periods, resulting in slightly positive CO_2 fluxes, probably due to increased microbial respiration in the drier, more aerated sediments. From a methodological point of view, the Random Forest model developed for this study explained 62% of total fluxes variability. The remaining 38% of variability could not be explained by either PAR, air temperature, relative humidity, wind speed, wind direction, air pressure or water levels. Comparing model predicted fluxes and measured fluxes, it appeared that during neap low tides, the model tended to over-estimated fluxes and by contrast at spring low tide, the model tended to under-estimated fluxes (Annex 6). In that case, the model could potentially highlight the irrigation effect on mudflat CO_2 uptake, which was not an explanatory variable considered in the model construction.

At immersion during all seasons, EC measurements from the mud zone were systematically negative, suggesting that the water column acted as a CO_2 sink during high tide whatever the season. Variability in the measured sink at immersion was also present, with the greatest CO_2 uptake occurring in summer (-1.53 ± 1.88 µmol m^{-2} s^{-1}), followed by winter (-0.82 ± 2.04 µmol m^{-2} s^{-1}), spring (-0.74 ± 1.34 µmol m^{-2} s^{-1}) and autumn (-0.27 ± 2.06 µmol m^{-2} s^{-1}). In contrast, calculated fluxes from pCO_2 values were positive for all seasons, indicating that CO_2 oversaturated waters released CO_2 to the atmosphere, with the highest release occurring in summer (0.49 ± 0.52 µmol m^{-2} s^{-1}) and the lowest in autumn (0.20 ± 0.24 µmol m^{-2} s^{-1}). The differences noticed between water-air EC fluxes and water pCO_2 measurement-based calculated fluxes highlighted the complexity of CO_2 exchange processes at the water-atmosphere interface, and associated biogeochemical heterogeneity in water mass bodies over tidal systems as the studied site. Indeed, EC measurements covered a large spatial area of water in the EC footprint depending on wind directions, whereas water pCO_2 measurements and flux calculations were made at a single point only. Further research at our site is then needed to better account for this water-air flux variability associated to water mass heterogeneity according to methodology, for instance improving emersion and immersion period definition or measuring water pCO_2 at different points. As the study area was rarely submerged, the influence of water on the overall annual carbon budget remained relatively limited. However, on shorter time scales, tidal immersion played an important role as observed over other tidal marsh or bay systems (Polsenaere et al. 2012; Mayen et al. 2024).

4.5. Carbon budget of the studied tidal marsh system

The intertidal mudflat of the Aiguillon Bay plays a complex and crucial role from a regional carbon budget point of view among the land-sea continuum formed by the Marais poitevin watershed and the Aiguillon bay communicating with the coastal ocean, as shown in Fig. 13, presenting the first integration of the different carbon export and flux data obtained in the previous and present studies at the different involved interfaces, time scales and methods. First, it shows that the uptake of atmospheric CO_2 by the whole studied system is strongly influenced by the dynamic interaction between the marsh and mudflat habitat zones, each contributing differently to the overall carbon flux. Over 2023 and over the whole bay of Aiguillon tidal marsh system, a net CO_2 uptake of -285 gC m^{-2} yr^{-1} (-10.5 tCO_2 eq. ha^{-1} yr^{-1}) was measured. Specifically, these large-scale EC measurements indicate a net uptake of CO_2 by the mud habitat, of -430 gC m^{-2} yr^{-1} (-15.8 tCO_2 eq. ha^{-1} yr^{-1}), which significantly exceeds the uptake capacity of the adjacent marsh zone, of -156 gC m^{-2} yr^{-1} (-5.7 tCO_2 eq. ha^{-1} yr^{-1}). This marsh uptake value is lower than the uptake capacity measured at 483 gC m^{-2} yr^{-1} in 2020 in a nearby marsh system (Mayen et al. 2024). Moreover, this marsh sink value (-5.7 tCO_2 eq. ha^{-1} yr^{-1}) is lower than the carbon sequestration (8.8 tCO_2 eq. ha^{-1} yr^{-1}) measured on the marsh zone of the bay by Amann et al. (2023). It highlights the role of horizontal carbon inputs from the adjacent terrestrial and coastal oceanic systems contributing to the carbon budget of the continuum. Indeed, carbon export rates from the Marais poitevin watershed to the bay in 2017-2018 was estimated at 7.2-22.2 gC m^{-2} an^{-1} (0.26-0.81 tCO_2 eq. ha^{-1} yr^{-1}) (Coignot et al. 2020; in prep.). Moreover, on the watershed, EC atmospheric CO_2 fluxes simultaneously measured over the freshwater marsh covered by agricultural lands, meadows and water canals gave a net CO_2 uptake of -59 gC m^{-2} yr^{-1} (-2.2 tCO_2 eq. ha^{-1} yr^{-1}). Carbon exchanges between the bay and the coastal ocean need to be address but coastal carbon inputs to the bay are certainly important since allochthonous sediments of marine origin dominated the signature of chemically-stable OC of marsh sediments at the studied tidal marsh system (Amann et al. 2023). Small scale CO_2 fluxes (diurnal/tidal) and underlying processes occurring in and between the different compartments (sediment, soil, water, atmosphere) and habitats play a significant role in the

carbon budget and such measurements need to be continued to better specify this regional budget in the context of climate change.

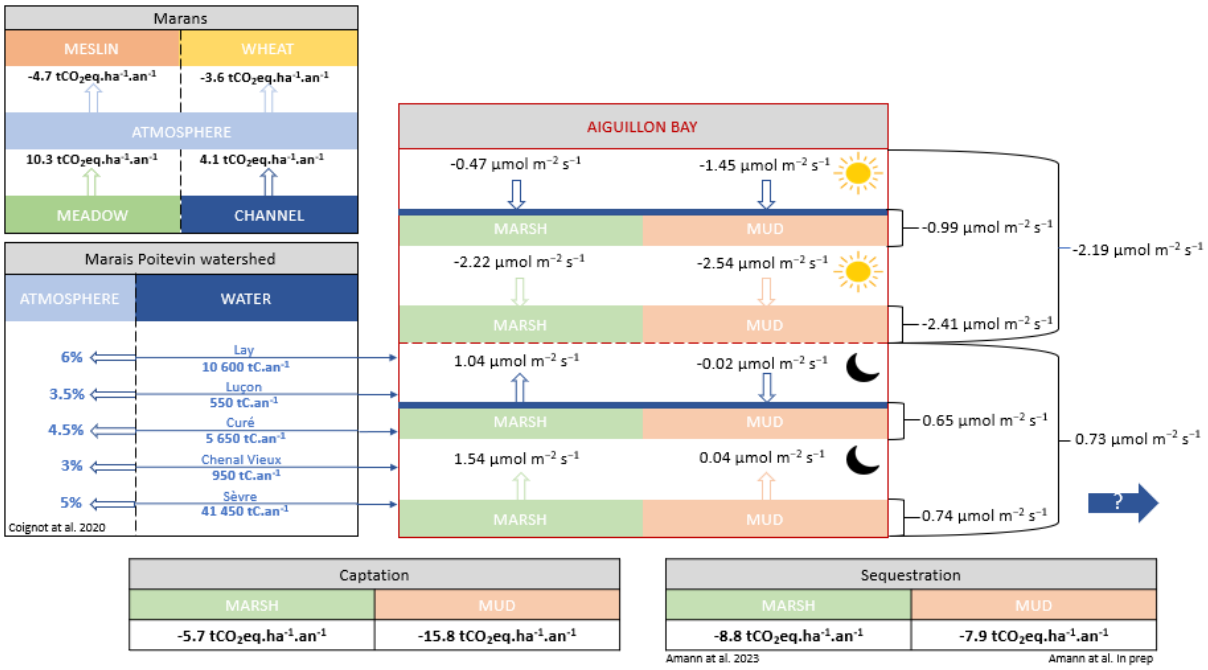

Figure 13. Regional Carbon Budget of the land-sea continuum formed by the Marais poitevin watershed – Aiguillon bay system. Terrestrial Carbon export and associated CO_2 degassing (years of 2017-2018) is shown (see Coignot et al. 2020; in prep.), along with simultaneous (2023-2024) atmospheric CO_2 fluxes measured by the LRTZC EC stations (Marans and Aiguillon bay (this study) stations), and carbon sequestration data from Amann et al. (2023 and in prep.). Smaller scale diurnal/tidal fluxes are also presented in the figure. The thick blue arrow indicates the export of C from the bay to the ocean (not yet studied).

BIBLIOGRAHIE

Amann, B., E. Chaumillon, S. Schmidt, L. Olivier, J. Jupin, M. C. Perello, et J. P. Walsh. 2023. « Multi-annual and multi-decadal evolution of sediment accretion in a saltmarsh of the French Atlantic coast: Implications for carbon sequestration ». *Estuarine, Coastal and Shelf Science* 293 (octobre):108467. https://doi.org/10.1016/j.ecss.2023.108467.

Baldocchi, Dennis D. 2003. « Assessing the Eddy Covariance Technique for Evaluating Carbon Dioxide Exchange Rates of Ecosystems: Past, Present and Future ». *Global Change Biology* 9 (4): 479-92. https://doi.org/10.1046/j.1365-2486.2003.00629.x.

Barr, A. G., A. D. Richardson, D. Y. Hollinger, D. Papale, M. A. Arain, T. A. Black, G. Bohrer, et al. 2013. « Use of change-point detection for friction–velocity threshold evaluation in eddy-covariance studies ». *Agricultural and Forest Meteorology* 171-172 (avril):31-45. https://doi.org/10.1016/j.agrformet.2012.11.023.

Bauer, James E., Wei-Jun Cai, Peter A. Raymond, Thomas S. Bianchi, Charles S. Hopkinson, et Pierre A. G. Regnier. 2013. « The Changing Carbon Cycle of the Coastal Ocean ». *Nature* 504 (7478): 61-70. https://doi.org/10.1038/nature12857.

Berg, Peter, Marie Lise Delgard, Pierre Polsenaere, Karen J. McGlathery, Scott C. Doney, et Amelie C. Berger. 2019. « Dynamics of Benthic Metabolism, O2, and pCO2 in a Temperate Seagrass Meadow ». *Limnology and Oceanography* 64 (6): 2586-2604. https://doi.org/10.1002/lno.11236.

Borges, A. V., B. Delille, et M. Frankignoulle. 2005. « Budgeting Sinks and Sources of CO2 in the Coastal Ocean: Diversity of Ecosystems Counts ». *Geophysical Research Letters* 32 (14). https://doi.org/10.1029/2005GL023053.

Borges, Alberto Vieira, et Michel Frankignoulle. 2003. « Distribution of Surface Carbon Dioxide and Air-Sea Exchange in the English Channel and Adjacent Areas ». *Journal of Geophysical Research: Oceans* 108 (C5). https://doi.org/10.1029/2000JC000571.

Breiman, Leo. 2001. « Random Forests ». *Machine Learning* 45 (1): 5-32. https://doi.org/10.1023/A:1010933404324.

Burba, George. 2013. *Eddy Covariance Method for Scientific, Industrial, Agricultural and Regulatory Applications: A Field Book on Measuring Ecosystem Gas Exchange and Areal Emission Rates*. https://doi.org/10.13140/RG.2.1.4247.8561.

Cahoon, Lawrence B. 1999. « THE ROLE OF BENTHIC MICROALGAE IN NERITIC ECOSYSTEMS ». In *Oceanography and Marine Biology*. CRC Press.

Cai, Wei-Jun. 2011. « Estuarine and Coastal Ocean Carbon Paradox: CO 2 Sinks or Sites of Terrestrial Carbon Incineration? » *Annual review of marine science* 3 (janvier):123-45. https://doi.org/10.1146/annurev-marine-120709-142723.

Cai, Wei-Jun, Minhan Dai, et Yongchen Wang. 2006. « Air-Sea Exchange of Carbon Dioxide in Ocean Margins: A Province-Based Synthesis ». *Geophysical Research Letters* 33 (12). https://doi.org/10.1029/2006GL026219.

Callaway, John C., et Michael N. Josselyn. 1992. « The Introduction and Spread of Smooth Cordgrass (Spartina Alterniflora) in South San Francisco Bay ». *Estuaries* 15 (2): 218-26. https://doi.org/10.2307/1352695.

Chen, C.-T. A., T.-H. Huang, Y.-C. Chen, Y. Bai, X. He, et Y. Kang. 2013. « Air–Sea Exchanges of CO_2 in the World's Coastal Seas ». *Biogeosciences* 10 (10): 6509-44. https://doi.org/10.5194/bg-10-6509-2013.

Chen, Jie, Dongqi Wang, Yangjie Li, Zhongjie Yu, Shu Chen, Xiyong Hou, John R. White, et Zhenlou Chen. 2020. « The Carbon Stock and Sequestration Rate in Tidal Flats From Coastal China ». *Global Biogeochemical Cycles* 34 (11): e2020GB006772. https://doi.org/10.1029/2020GB006772.

Chen, Zhao Liang, et Shing Yip Lee. 2022. « Tidal Flats as a Significant Carbon Reservoir in Global Coastal Ecosystems ». *Frontiers in Marine Science* 9 (mai). https://doi.org/10.3389/fmars.2022.900896.

Chmura, Gail L. 2013. « What do we need to assess the sustainability of the tidal salt marsh carbon sink? » *Ocean & Coastal Management* 83 (octobre):25-31. https://doi.org/10.1016/j.ocecoaman.2011.09.006.

Christianen, M. J. A., J. J. Middelburg, S. J. Holthuijsen, J. Jouta, T. J. Compton, T. van der Heide, T. Piersma, et al. 2017. « Benthic Primary Producers Are Key to Sustain the Wadden Sea Food Web: Stable Carbon Isotope Analysis at Landscape Scale ». *Ecology* 98 (6): 1498-1512. https://doi.org/10.1002/ecy.1837.

Coignot, Elise, Pierre Polsenaere, Patrick Soletchnik, Olivier Le Moine, Philippe Souchu, Emmanuel Joyeux, Yoann Le Roy, et al. 2020. « Variabilité spatio-temporelle des nutriments et du carbone et flux associés le long d'un continuum terrestre-aquatique tempéré (Marais poitevin – Baie de l'Aiguillon – Pertuis Breton) ». *Archimer, archive institutionnelle de l'Ifremer*. Archimer, archive institutionnelle de l'Ifremer.

Cui, Xia, Thomas Goff, Song Cui, Dorothy Menefee, Qiang Wu, Nithya Rajan, Shyam Nair, Nate Phillips, et Forbes Walker. 2021. « Predicting carbon and water vapor fluxes using machine learning and novel feature ranking algorithms ». *Science of The Total Environment* 775 (juin):145130. https://doi.org/10.1016/j.scitotenv.2021.145130.

Duarte, Bernardo, João Carreiras, et Isabel Caçador. 2021. « Climate Change Impacts on Salt Marsh Blue Carbon, Nitrogen and Phosphorous Stocks and Ecosystem Services ». *Applied Sciences* 11 (4): 1969. https://doi.org/10.3390/app11041969.

Friedlingstein, Pierre, Michael O'Sullivan, Matthew W. Jones, Robbie M. Andrew, Dorothee C. E. Bakker, Judith Hauck, Peter Landschützer, et al. 2023. « Global Carbon Budget 2023 ». *Earth System Science Data* 15 (12): 5301-69. https://doi.org/10.5194/essd-15-5301-2023.

Gash, J. H. C., et A. D. Culf. 1996. « Applying a Linear Detrend to Eddy Correlation Data in Realtime ». *Boundary-Layer Meteorology* 79 (3): 301-6. https://doi.org/10.1007/BF00119443.

Gattuso, J.-P., M. Frankignoulle, et R. Wollast. 1998. « Carbon and Carbonate Metabolism in Coastal Aquatic Ecosystems ». *Annual Review of Ecology and Systematics* 29 (1): 405-34. https://doi.org/10.1146/annurev.ecolsys.29.1.405.

Godet, Laurent, Laurent Pourinet, Emmanuel Joyeux, et Fernand Verger. 2015. « Dynamique spatiale et usage des schorres de l'Anse de l'Aiguillon de 1705 à nos jours. Enjeux de conservation d'un patrimoine naturel littoral marin ». *Cybergeo: European Journal of Geography*, février. https://doi.org/10.4000/cybergeo.26774.

Gu, Lianhong, Eva M. Falge, Tom Boden, Dennis D. Baldocchi, T. A. Black, Scott R. Saleska, Tanja Suni, et al. 2005. « Objective threshold determination for nighttime eddy flux filtering ». *Agricultural and Forest Meteorology* 128 (3): 179-97. https://doi.org/10.1016/j.agrformet.2004.11.006.

Hancke, Kasper, et Ronnie N. Glud. 2004. « Temperature Effects on Respiration and Photosynthesis in Three Diatom-Dominated Benthic Communities ». *Aquatic Microbial Ecology* 37 (3): 265-81. https://doi.org/10.3354/ame037265.

Herlory, O., J.-M. Guarini, P. Richard, et G. F. Blanchard. 2004. « Microstructure of Microphytobenthic Biofilm and Its Spatio-Temporal Dynamics in an Intertidal Mudflat (Aiguillon Bay, France) ». *Marine Ecology Progress Series* 282 (novembre):33-44. https://doi.org/10.3354/meps282033.

« Influence of Typology and Management Practices on Water pCO2 and Atmospheric CO2 Fluxes over Two Temperate Shelf–Estuary–Marsh Water Continuums ». 2023.

Regional Studies in Marine Science 67 (décembre):103209. https://doi.org/10.1016/j.rsma.2023.103209.

Intergovernmental Panel on Climate Change (IPCC), éd. 2023. « Global Carbon and Other Biogeochemical Cycles and Feedbacks ». In *Climate Change 2021 – The Physical Science Basis: Working Group I Contribution to the Sixth Assessment Report of the Intergovernmental Panel on Climate Change*, 673-816. Cambridge: Cambridge University Press. https://doi.org/10.1017/9781009157896.007.

Kathilankal, James C., Thomas J. Mozdzer, Jose D. Fuentes, Paolo D'Odorico, Karen J. McGlathery, et Jay C. Zieman. 2008. « Tidal Influences on Carbon Assimilation by a Salt Marsh ». *Environmental Research Letters* 3 (4): 044010. https://doi.org/10.1088/1748-9326/3/4/044010.

Kim, Yeonuk, Mark S. Johnson, Sara H. Knox, T. Andrew Black, Higo J. Dalmagro, Minseok Kang, Joon Kim, et Dennis Baldocchi. 2020. « Gap-Filling Approaches for Eddy Covariance Methane Fluxes: A Comparison of Three Machine Learning Algorithms and a Traditional Method with Principal Component Analysis ». *Global Change Biology* 26 (3): 1499-1518. https://doi.org/10.1111/gcb.14845.

Kritzer, Jacob P., Mari-Beth DeLucia, Emily Greene, Caroly Shumway, Marek F. Topolski, Jessie Thomas-Blate, Louis A. Chiarella, Kay B. Davy, et Kent Smith. 2016. « The Importance of Benthic Habitats for Coastal Fisheries ». *BioScience* 66 (4): 274-84. https://doi.org/10.1093/biosci/biw014.

Laruelle, G. G., H. H. Dürr, R. Lauerwald, J. Hartmann, C. P. Slomp, N. Goossens, et P. a. G. Regnier. 2013. « Global Multi-Scale Segmentation of Continental and Coastal Waters from the Watersheds to the Continental Margins ». *Hydrology and Earth System Sciences* 17 (5): 2029-51. https://doi.org/10.5194/hess-17-2029-2013.

Laruelle, Goulven G., Hans H. Dürr, Caroline P. Slomp, et Alberto V. Borges. 2010. « Evaluation of Sinks and Sources of CO2 in the Global Coastal Ocean Using a Spatially-Explicit Typology of Estuaries and Continental Shelves ». *Geophysical Research Letters* 37 (15). https://doi.org/10.1029/2010GL043691.

Laurila, Tuomas, Mika Aurela, et Juha-Pekka Tuovinen. 2012. « Eddy Covariance Measurements over Wetlands ». In *Eddy Covariance: A Practical Guide to Measurement and Data Analysis*, édité par Marc Aubinet, Timo Vesala, et Dario Papale, 345-64. Dordrecht: Springer Netherlands. https://doi.org/10.1007/978-94-007-2351-1_14.

Lee, Li-Hua, Li-Yung Hsieh, et Hsing-Juh Lin. 2011. « In Situ Production and Respiration of the Benthic Community during Emersion on Subtropical Intertidal Sandflats ». *Marine Ecology Progress Series* 441 (novembre):33-47. https://doi.org/10.3354/meps09362.

Li, Bo, Chengz-hang Liao, Xiao-dong Zhang, Hui-li Chen, Qing Wang, Zhong-yi Chen, Xiao-jing Gan, et al. 2009. « *Spartina alterniflora* invasions in the Yangtze River estuary, China: An overview of current status and ecosystem effects ». *Ecological Engineering*, Wetland restoration and ecological engineering, 35 (4): 511-20. https://doi.org/10.1016/j.ecoleng.2008.05.013.

Liaw, Andy, et Matthew Wiener. 2002. « Classification and regression by randomForest ». *R News* 2 (3): 18-22.

MacIntyre, Hugh L., Richard J. Geider, et Douglas C. Miller. 1996. « Microphytobenthos: The Ecological Role of the "Secret Garden" of Unvegetated, Shallow-Water Marine Habitats. I. Distribution, Abundance and Primary Production ». *Estuaries* 19 (2): 186-201. https://doi.org/10.2307/1352224.

Macreadie, Peter I., Micheli D. P. Costa, Trisha B. Atwood, Daniel A. Friess, Jeffrey J. Kelleway, Hilary Kennedy, Catherine E. Lovelock, Oscar Serrano, et Carlos M. Duarte.

2021. « Blue Carbon as a Natural Climate Solution ». *Nature Reviews Earth & Environment* 2 (12): 826-39. https://doi.org/10.1038/s43017-021-00224-1.

Macreadie, Peter I., A. Randall Hughes, et David L. Kimbro. 2013. « Loss of 'Blue Carbon' from Coastal Salt Marshes Following Habitat Disturbance ». *PLOS ONE* 8 (7): e69244. https://doi.org/10.1371/journal.pone.0069244.

Mayen, J., P. Polsenaere, É. Lamaud, M. Arnaud, P. Kostyrka, J.-M. Bonnefond, P. Geairon, et al. 2024. « Atmospheric CO2 exchanges measured by eddy covariance over a temperate salt marsh and influence of environmental controlling factors ». *Biogeosciences* 21 (4): 993-1016. https://doi.org/10.5194/bg-21-993-2024.

Mayen, Jérémy, Pierre Polsenaere, Aurore Regaudie de Gioux, Christine Dupuy, Marie Vagner, Jean-Christophe Lemesle, Benoit Poitevin, et Philippe Souchu. 2023. « Influence of typology and management practices on water pCO2 and atmospheric CO2 fluxes over two temperate shelf–estuary–marsh water continuums ». *Regional Studies in Marine Science* 67 (décembre):103209. https://doi.org/10.1016/j.rsma.2023.103209.

Mcleod, Elizabeth, Gail L Chmura, Steven Bouillon, Rodney Salm, Mats Björk, Carlos M Duarte, Catherine E Lovelock, William H Schlesinger, et Brian R Silliman. 2011. « A Blueprint for Blue Carbon: Toward an Improved Understanding of the Role of Vegetated Coastal Habitats in Sequestering CO2 ». *Frontiers in Ecology and the Environment* 9 (10): 552-60. https://doi.org/10.1890/110004.

Mcowen, Chris J, Lauren V Weatherdon, Jan-Willem Van Bochove, Emma Sullivan, Simon Blyth, Christoph Zockler, Damon Stanwell-Smith, et al. 2017. « A global map of saltmarshes ». *Biodiversity Data Journal*, n° 5 (mars), e11764. https://doi.org/10.3897/BDJ.5.e11764.

Méléder, Vona, Raphael Savelli, Alexandre Barnett, Pierre Polsenaere, Pierre Gernez, Philippe Cugier, Astrid Lerouxel, et al. 2020. « Mapping the Intertidal Microphytobenthos Gross Primary Production Part I: Coupling Multispectral Remote Sensing and Physical Modeling ». *Frontiers in Marine Science* 7. https://www.frontiersin.org/articles/10.3389/fmars.2020.00520.

Mendelssohn, Irving A., et James T. Morris. 2002. « Eco-Physiological Controls on the Productivity of Spartina Alterniflora Loisel ». In *Concepts and Controversies in Tidal Marsh Ecology*, édité par Michael P. Weinstein et Daniel A. Kreeger, 59-80. Dordrecht: Springer Netherlands. https://doi.org/10.1007/0-306-47534-0_5.

Migné, A., D. Davoult, N. Spilmont, D. Menu, G. Boucher, J.-P. Gattuso, et H. Rybarczyk. 2002a. « A Closed-Chamber CO2-Flux Method for Estimating Intertidal Primary Production and Respiration under Emersed Conditions ». *Marine Biology* 140 (4): 865-69. https://doi.org/10.1007/s00227-001-0741-1.

———. 2002b. « A Closed-Chamber CO2-Flux Method for Estimating Intertidal Primary Production and Respiration under Emersed Conditions ». *Marine Biology* 140 (4): 865-69. https://doi.org/10.1007/s00227-001-0741-1.

Migné, A., N. Spilmont, G. Boucher, L. Denis, C. Hubas, M. -A. Janquin, M. Rauch, et D. Davoult. 2009. « Annual budget of benthic production in Mont Saint-Michel Bay considering cloudiness, microphytobenthos migration, and variability of respiration rates with tidal conditions ». *Continental Shelf Research* 29 (19): 2280-85. https://doi.org/10.1016/j.csr.2009.09.004.

Migné, A., N. Spilmont, et D. Davoult. 2004. « In situ measurements of benthic primary production during emersion: seasonal variations and annual production in the Bay of Somme (eastern English Channel, France) ». *Continental Shelf Research* 24 (13): 1437-49. https://doi.org/10.1016/j.csr.2004.06.002.

Morris, James T., Karen Sundberg, et Charles S. Hopkinson. 2013. « Salt Marsh Primary Production and Its Responses to Relative Sea Level and Nutrients in Estuaries at Plum

Island, Massachusetts, and North Inlet, South Carolina, USA ». *Oceanography* 26 (3): 78-84.
Ouisse, Vincent, Aline Migné, et Dominique Davoult. 2011. « Community-Level Carbon Flux Variability over a Tidal Cycle in Zostera Marina and Z. Noltii Beds ». *Marine Ecology Progress Series* 437:79-87. https://doi.org/10.3354/meps09274.
Papale, D., M. Reichstein, M. Aubinet, E. Canfora, C. Bernhofer, W. Kutsch, B. Longdoz, et al. 2006. « Towards a standardized processing of Net Ecosystem Exchange measured with eddy covariance technique: algorithms and uncertainty estimation ». *Biogeosciences* 3 (4): 571-83. https://doi.org/10.5194/bg-3-571-2006.
Polsenaere, Pierre. 2011. « Echanges de CO2 atmosphérique dans la lagune d'Arcachon et relations avec le métabolisme intertidal ». These de doctorat, Bordeaux 1. https://www.theses.fr/2011BOR14253.
Polsenaere, Pierre, Jonathan Deborde, Guillaume Detandt, Luciana O. Vidal, Marcela A. P. Pérez, Vincent Marieu, et Gwenaël Abril. 2013. « Thermal Enhancement of Gas Transfer Velocity of CO2 in an Amazon Floodplain Lake Revealed by Eddy Covariance Measurements ». *Geophysical Research Letters* 40 (9): 1734-40. https://doi.org/10.1002/grl.50291.
Polsenaere, Pierre, Bruno Delille, Dominique Poirier, Céline Charbonnier, Jonathan Deborde, Aurélia Mouret, et Gwenaël Abril. 2023. « Seasonal, Diurnal, and Tidal Variations of Dissolved Inorganic Carbon and pCO2 in Surface Waters of a Temperate Coastal Lagoon (Arcachon, SW France) ». *Estuaries and Coasts* 46 (1): 128-48. https://doi.org/10.1007/s12237-022-01121-6.
Polsenaere, Pierre, Eric Lamaud, Virginie Lafon, Jean-Marc J.-M. Bonnefond, Patrice Bretel, Bruno Delille, Jonathan Deborde, Denis Loustau, et Gwenaël Abril. 2012. « Spatial and Temporal CO2 Exchanges Measured by Eddy Covariance over a Temperate Intertidal Flat and Their Relationships to Net Ecosystem Production ». *Biogeosciences* 9 (1): 249. https://doi.org/10.5194/bg-9-249-2012.
Regnier, Pierre, Pierre Friedlingstein, Philippe Ciais, Fred T. Mackenzie, Nicolas Gruber, Ivan A. Janssens, Goulven G. Laruelle, et al. 2013. « Anthropogenic Perturbation of the Carbon Fluxes from Land to Ocean ». *Nature Geoscience* 6 (8): 597-607. https://doi.org/10.1038/ngeo1830.
Reynolds. 1886. « I. On the Theory of Lubrication and Its Application to Mr. Beauchamp Tower's Experiments, Including an Experimental Determination of the Viscosity of Olive Oil ». *Proceedings of the Royal Society of London* 40 (242-245): 191-203. https://doi.org/10.1098/rspl.1886.0021.
Rigaud, S., B. Deflandre, O. Maire, G. Bernard, J. C. Duchêne, D. Poirier, et P. Anschutz. 2018. « Transient biogeochemistry in intertidal sediments: New insights from tidal pools in *Zostera noltei* meadows of Arcachon Bay (France) ». *Marine Chemistry* 200 (mars):1-13. https://doi.org/10.1016/j.marchem.2018.02.002.
Roobaert, Alizée, Goulven G. Laruelle, Peter Landschützer, Nicolas Gruber, Lei Chou, et Pierre Regnier. 2019. « The Spatiotemporal Dynamics of the Sources and Sinks of CO2 in the Global Coastal Ocean ». *Global Biogeochemical Cycles* 33 (12): 1693-1714. https://doi.org/10.1029/2019GB006239.
Savelli, Raphaël, Christine Dupuy, Laurent Barillé, Astrid Lerouxel, Katell Guizien, Anne Philippe, Pierrick Bocher, Pierre Polsenaere, et Vincent Le Fouest. 2018. « On Biotic and Abiotic Drivers of the Microphytobenthos Seasonal Cycle in a Temperate Intertidal Mudflat: A Modelling Study ». *Biogeosciences* 15 (23): 7243-71. https://doi.org/10.5194/bg-15-7243-2018.
Spilmont, N., D. Davoult, et A. Migné. 2006. « Benthic Primary Production during Emersion: In Situ Measurements and Potential Primary Production in the Seine Estuary (English

Channel, France) ». *Marine Pollution Bulletin*, Recent Developments in Estuarine Ecology and Management, 53 (1): 49-55. https://doi.org/10.1016/j.marpolbul.2005.09.016.

Van Dam, Bryce, Pierre Polsenaere, Aylin Barreras-Apodaca, Christian Lopes, Zulia Sanchez-Mejia, Tatsuki Tokoro, Tomohiro Kuwae, et al. 2021. « Global Trends in Air-Water CO2 Exchange Over Seagrass Meadows Revealed by Atmospheric Eddy Covariance ». *Global Biogeochemical Cycles* 35 (4): e2020GB006848. https://doi.org/10.1029/2020GB006848.

Vesala, T., N. Kljun, Ü. Rannik, J. Rinne, A. Sogachev, T. Markkanen, K. Sabelfeld, Th. Foken, et M. Y. Leclerc. 2008. « Flux and concentration footprint modelling: State of the art ». *Environmental Pollution* 152 (3): 653-66. https://doi.org/10.1016/j.envpol.2007.06.070.

Wang, Zhaohui Aleck, et Wei-Jun Cai. 2004. « Carbon Dioxide Degassing and Inorganic Carbon Export from a Marsh-Dominated Estuary (the Duplin River): A Marsh CO2 Pump ». *Limnology and Oceanography* 49 (2): 341-54. https://doi.org/10.4319/lo.2004.49.2.0341.

ANNEXES

Annex 1. Surface areas (in hectare) of each habitat within the EC footprint computed for each wind sectors. Underlined, the mean surface inside the 90% contour line of the wind sector and in bold the total surface of each habitat insight the 2023 mean footprint.

	ENE	ESE	SSE	SSW	NNE	NNW	WNW	WSW	Total
Agropyron	0	0	0.2	1.3	0	0	0	0	**1.6**
Agropyron	0	0.4	0	0.2	0	0	0	0	**0.6**
Aster	1.0	0.7	0.6	1.9	0	0	0	0	**4.1**
Halimione	5.3	6.1	4.5	2.7	0	0	0	0	**18.6**
Salicornia	0.8	0.4	0.7	0.6	0	0	0	0	**2.5**
Spartina	1.3	0.2	0.2	1.2	0	0	0	0	**2.8**
Phragmites	0	0	0.2	0.1	0	0	0	0	**0.3**
Mud	4.7	0.6	0.5	2.0	11.4	6.4	8.2	16.2	**50.1**
Channel	0.4	0	0	0	0.8	0.4	0.9	0.7	**3.2**
NA	0	0	0.2	0.4	0	0	0	1.3	**1.9**
Total	**13.4**	**8.3**	**7.3**	**10.3**	**12.2**	**6.8**	**9.2**	**18.3**	**85.8**

Annex 2. Different RF models trained on the data and their associated metrics (RMSE, R2 and bias). With relative humidity (RH), air temperature (Ta), wind direction (wd), wind speed (ws), air pressure (Pa) and water height (Hw).

	Variables	RMSE	R2	Bias
Model 1	PAR, RH, Ta, wd, Hw	2.21	0.49	-0.03
Model 2	PAR, RH, Ta, wd, ws, Pa	1.93	0.61	-0.02
Model 3	PAR, RH, Ta, wd, ws, Pa, Hw	1.90	0.63	-0.02
Model 4	PAR, RH, Ta, wd, Pa, Hw	1.94	0.61	-0.02
Model 5	PAR, RH, Ta, wd, ws, Hw	2.02	0.58	-0.03

Annex 3. Water pCO_2 sensor (C-SenseTM; PME/Turner Designs) associated with a multiparameter sensor (a) and a clear benthic chamber deployed on the mudflat (b)

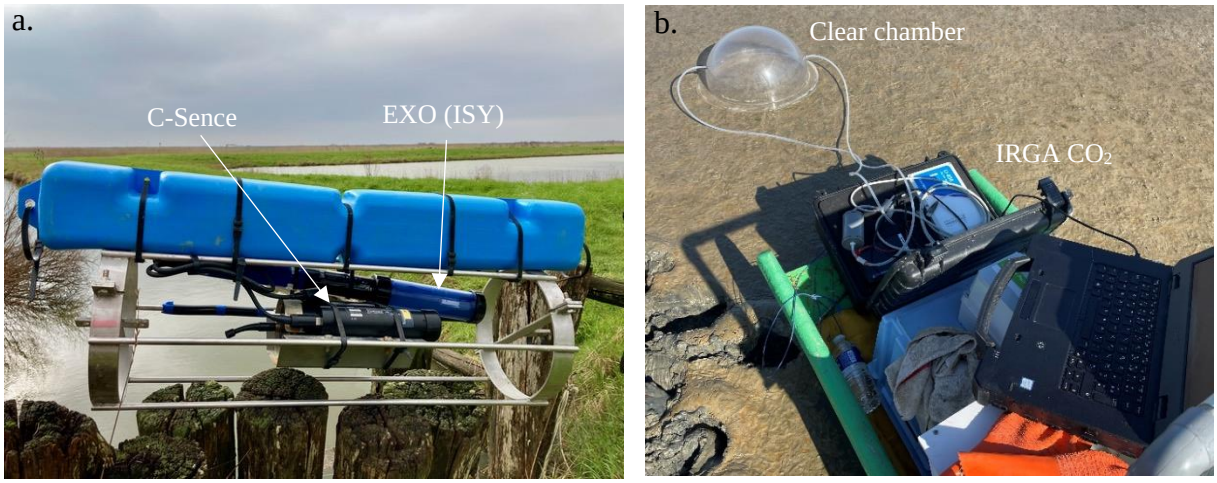

Annex 4. Daytime EC fluxes without dry and warm periods according to PAR values.

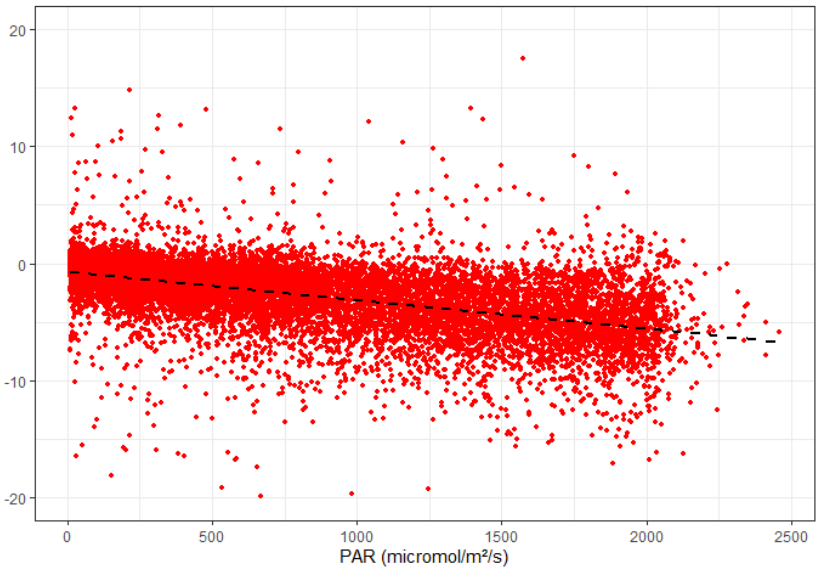

Annex 5. EC footprint estimation from daytime (a) or night-time (b) measurements.

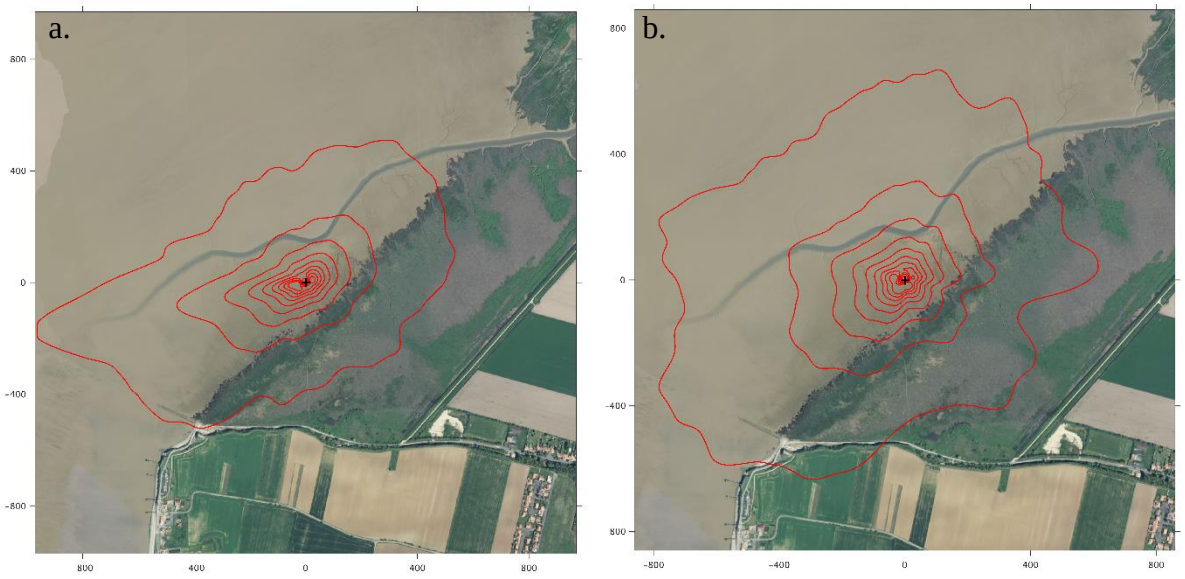

Annex 6. Variations in predicted (a) and measured (b) fluxes over the mudflat, water heights (c) and wind directions (d) over August.